UNIVERSITÉ DU QUÉBEC

MÉMOIRE PRÉSENTÉ À

L'UNIVERSITÉ DU QUÉBEC À CHICOUTIMI COMME

EXIGENCE PARTIELLE

DE LA MAÎTRISE EN INGÉNIERIE

BY

Ping Li

Safety analysis using a Smart Safety Helmet embedded with IMU and EEG sensors applied in industrial facility

August 2015

Abstract

Some mental states, such as fatigue, or sleepiness, are known to increase the potential of accidents in industry, and thus could decrease productivity, even increase cost for healthcare. The highest rate of industrial accidents is usually found among shift workers due to fatigue or extended work hours. When using machine tool or interacting with robotic system, the risk of injury increases due to disturbance, lapse in concentration, vigilance decline, and neglect of the risk during prolonged use.

Usually, to guarantee safety of worker, the conventional means is to stop the machine when human presence is detected in the safeguarding area of machine tool or robot workspace. The popular human detection technologies exploit laser scanner, camera (or motion tracker), infrared sensor, open-door sensor, static pressure sensitive floor as described in CSA Z434 standard. Of course, in the field of robotic, human and robot are not allowed to work together in the same workspace. However, new industrial needs lead research to develop flexible and reactive chain production for enabling small quantity production or fast modification in product characteristics. Consequently, more efficient human-machine or human-robot collaboration under a safety condition could improve this flexibility.

Our research project aims at detecting and analyzing human safety in industry in order to protect workers. Comparing to the conventional human protection methods, our research exploits Artificial Intelligence approach to track and monitor human head motion and mental state using an instrumented safety helmet, labelled as Smart Safety Helmet (SSH) in the following. The contribution of this thesis consists in the design of data fusion algorithm for the recognition of head motion and mental state, which can be used to analyze the potential risky states of workers. A Smart Safety Helmet embedded with Inertial Measurement Unit (IMU) and EEG sensors will be used to detect and decode the human's mental state and intention. The acquired information will be used to estimate the accident risk level in order to stop machine and then prevent accident or injury. In human-robot interaction (HRI) paradigm, the human's intention could be used to predict the worker trajectory in order to control the robot moving trajectory and then to avoid fatal collision.

Résumé

Certains états mentaux, comme la fatigue ou la somnolence, sont connus pour augmenter le potentiel d'accidents dans l'industrie, et pourrait donc réduire la productivité, même augmenter les coûts des soins de santé. Le taux le plus élevé d'accidents au travail est habituellement trouvé parmi les travailleurs en rotation (travail posté) dues à la fatigue ou les heures de travail prolongées. Lors de l'utilisation d'une machine-outil ou lors d'une interaction avec un système robotique, le risque de lésion peut augmenter dû à une perturbation, un manque de concentration, une baisse de vigilance et la négligence du travailleur face au risque présent lors d'une utilisation prolongée (accoutumance au risque).

Habituellement, pour garantir la sécurité des travailleurs, des moyens classiques sont l'arrêt complet de la machine lorsque la présence humaine est détectée dans une zone non sécuritaire, par exemple dans l'espace de travail d'un robot. Les technologies industrielles communes de détection humaine exploitent le scanner au laser, la caméra (par la capture de mouvement), le capteur infrarouge, l'interrupteur de porte ouverte, le tapis de capture de la pression statique ; tous ces capteurs sont décrits dans la norme CSA Z434. Jusqu'à tout récemment, dans le domaine de la robotique industrielle, les humains et les robots n'étaient pas autorisés à travailler ensemble dans le même espace. Toutefois, des besoins industriels émergents ont dirigé les recherches pour développer une production flexible et réactive pour favoriser la production de petites quantités ou modifier rapidement des caractéristiques du produit. Par conséquent, une collaboration plus efficace entre l'humain et le robot ou, de manière plus générale entre l'humain et la machine, sous des contraintes de sécurité, pourrait améliorer cette flexibilité et cette réactivité.

Notre projet de recherche vise à détecter et à analyser la sécurité humaine dans l'industrie afin de protéger les travailleurs. En comparant les méthodes classiques de protection humaine, notre approche exploite l'intelligence artificielle pour identifier les mouvements de la tête et identifier l'état mental en utilisant un casque de sécurité instrumenté, nommé le Smart Safety Helmet (SSH) dans ce qui suit. La contribution de ce mémoire réside dans la conception de la fusion des données provenant de la reconnaissance de mouvement de la tête et de l'état mental, qui peut être utilisée pour analyser le potentiel de risque encouru par un travailleur. Dans le SSH, une unité de mesure inertielle (IMU) et capteurs EEG ont été intégrés. Ces deux capteurs seront utilisés pour détecter l'état mental de l'humain et décoder son intention. Les informations recueillies seront utilisées pour estimer le risque d'accidents afin d'arrêter la machine et d'empêcher un accident. Dans le paradigme de l'interaction humain-robot, l'intention de l'humain pourrait être utilisée modifier le comportement du robot (réduire sa rigidité ou modifier sa trajectoire).

Acknowledgements

I would like to thank hearty **Prof. M. Martin Otis**, my director for his support, supervision, guidance, encouragement, motivation and patience in this research. I will forever be indebted to you for showing your interest, generous help during my Masters' studies. Special thanks to **Prof. M. Hassan Ezzaidi**, my co-director and mentor for his patience and guidance. I am particularly grateful for all of your time and help during last two years.

I would like to show my deepest appreciations to all of my friends and collaborators who provided assistance in LAIMI Laboratory of the University of Quebec at Chicoutimi (UQAC). Special thanks to technicians, for all their collaborations.

Finally, I would like to thank my family, especially Huiwei Zhao, my wife. Thank you for your accompanying and endurance support. I love my children, Changyu and Chancie.

Table of Contents

List of Figures

List of Tables

List of Abbreviation

IMU,	Inertial Measurement Unit
SSH,	Smart Safety Helmet
EEG,	Electroencephalogram
EOG,	Electrooculography
EMG,	Electromyogram
pHRI,	physical human robot interaction
MLP,	Multi-layer perceptron
ANN,	Artificial Neural Network
CSA,	Canadian Standards Association

Chapter 1: Introduction

In traditional industrial facility, operator usually needs to interact with machinery, such as drill, cutter, which requires the operator to pay more attention during the process, because negligence may cause injury to the operator.

During past decades, industrial automation trend has introduced a large number of robots in order to replace human workers to perform dangerous, difficult tasks and improve production efficiency. These robots can produce powerful and rapid movements through a working cell. As a result, the hazard threats to human is increased when human is working surrounding the robot or interacting with the robot (physical human-robot interaction), because the human's trajectory is unpredictable and unavailable for the robots [1].

In this chapter, we will discuss the human safety issue in industry. Then, the project strategy of this research is presented.

1.1 Human safety in industry

Investigations in Japan indicate that more than 50% of working accidents with robots can be attributed to faults in the electronic circuits of the control system; meanwhile, "human error" was responsible for less than 20% [2]. In Canada, the work related injury statistics indicates that the highest injury number occurs at the occupation "Trades and skilled transport and equipment operators", which take 30% of the total number of fatalities between 2011 and 2013 [3]. These researches indicate that real time monitor of the human states surrounding the robot or the equipment is necessary for collision avoidance and injury reduction. Collision avoidance, accidents and injury research already became an important aspect in robotics field for human safety [1, 4].

There are many methods of preventing industrial injuries, including prediction of problems by risk assessment, safety training, personal protective safety guards, mechanisms on machinery, and safety barriers. Usually, the conventional means of human protection is to emergently stop the machine when human is detected in the risky area of machine tool or enter the safeguard area of a robot. The popular technologies of human detection usually exploit laser scanner, camera (or motion tracker), infrared sensor, open-door sensor, static pressure sensitive floor and passive capacitive change sensing as described in CSA Z434

standard. Of course, in the field of robotic, human and robot are usually not allowed to work together in the same workspace [5, 6]. Special care should be exercised where an operator is required to interact with the robot on each operating cycle, such as to feed parts to the robot for processing [7]. When a human is found in the reachable workspace of the end-effector of the robot, it is usually stopped, which ends production.

However, new industrial needs lead research to develop flexible and reactive chain production for enabling small quantity production or fast modification in product characteristics [8]. Consequently, more efficient human-machine or human-robot collaboration (usually sharing a common work cell) under a safety condition could improve this flexibility since the future robots, especially for cooperative work, is expected to interact with human more directly [9].

On the other hand, in industrial environment, repeated working activities, noise level, and shift change could affect the operator physiological status, mental states and then possibly result in fatigue, lack of concentration, vigilance decline, and sleepiness. Abnormal physiological statuses, such as fatigue or drowsiness, are known as potential threats to the human health and factors of accidents. The highest rate of industrial accidents is usually found among shift workers due to fatigue or extended work hours [10]. Meanwhile, fatigue levels are not easily quantified; therefore it is difficult to identify the effect of these mental states on accident and injury rates. However, fatigue is still considered as a contributing factor with 20% in reported accidents and incidents across all sectors in industry [11]. Consequently, monitoring the mental states of operators could identify the potential risk, and be helpful to prevent the accident.

1.2 Project strategy

Our research project aims at detecting and analyzing the human safety in industry using an intelligent approach in order to protect workers. Comparing to the conventional human protection methods, our research exploits Artificial Intelligence approach to track and monitor human head motion and mental state using an instrumented safety helmet, labelled Smart Safety Helmet in the following. Human mental states and intention could be reflected in brainwave and head motion, so monitoring the mental states and head motion may determine whether or not a worker is involved in potential risk in an industrial facility.

Previous researches have indicated that information regarding mental states, such as vigilance, sleep, awake, could be reflected in the EEG record soon and accurately [12, 13]. It has been observed that a decrease in the level of vigilance could be represented by an increase in theta (θ) and alpha (α) bands activity, in contrast with a decrease in beta (β) band activity from the EEG power spectra [14-16]. In practice, monitoring theta (θ), alpha (α) and beta (β) bands activities could determine if mental state is transiting from alert to non-alert which could increase the potential risk level of accident [17]. As well, the eye blink has been proposed to be a suitable indicator for mental fatigue evaluation [18-20]. And it could be extracted from EEG measurement since it has high amplitude comparing to normal brain EEG signal. Detecting and analyzing of the EEG signal could extract relavent brainwave parameter in order to determine the vigilance level. In a workplace, a detection of vigilance decline means the increase of risk level of a potential accident.

There should be two steps to involve head gestures tracking in human safety protection. First of all, it is necessary to identify the risky head motion, such as nodding off caused by drowsiness, because these head motions indicate or represent the dangerous status to worker in an industrial environment. The second step is to differentiate and recognize different head gestures (yes, no, look up and down), orientation and some activities (walking, turning and climbing). The risk level of these gestures should be considered according to the combination of relevant workplace.

When an operator is working around a rotating machine, such as a drill, he should stare at the drill bit and keep vigilant. Wearing the SSH, when head motion is not recognized as the correct gesture from watching the machine tool, it should be considered as an increase of the risk level consequently to convey an alert to the operator. Furthermore, if the EEG sensors detect a drowsiness signal, the risk level should increase enough in order to shut down the tool and avoid accident. Thereby, signals coming from both IMU and EEG should be fused in order to evaluate a risk level of accident.

In pHRI (human-robot interaction) scenario, monitoring a worker’s head orientation is an important step towards safe cooperation, since head orientation is related to a worker’s direction of attention. Head gesture could be used to extract the real time head orientation, which could determine if the worker is staring at the robot during working. As well, the

EEG monitoring could determine if the worker is keeping vigilant and concentrated during pHRI.

The contribution of this thesis consists in exploring the algorithm for the recognition of head motion and mental state which can be used to analyze the potential risky state of workers. A Smart Safety Helmet embedded with Inertial Measurement Unit (IMU) and EEG sensors will be used to detect and decode human's mental state and intention. The acquired information will be used to estimate the accident risk level in order to stop machine and then prevent accident or injury. In pHRI paradigm, the human's intention could be used to predict the worker trajectory in order to control the robot moving trajectory to avoid fatal collision.

A literature review of motion measurement, gesture recognition algorithm, and EEG based drowsiness detection is first presented in order to understand the context of this research in the Chapter 2. Chapter 3 will present the suggested hardware and software developed for this research. Then, we will present the head motion identification using IMU in Chapter 4 and 5. The eye blink extraction from EEG will be explained in Chapter 6. Finally, we discuss the achieved result and present future works for this project.

Chapter 2: Literature Review

In an industrial environment, the most critical requirement is to guarantee the operator safety to reduce the work related injury, especially in human-machine interaction and pHRI. Conventional human protection methods usually prevent access into the safeguarded space by use of interlocked barriers, or stop the machine by human-presence-sensing safeguarding devices, such as area scanning or capacitance-sensing safeguarding systems. Normally, these systems are effective, but expensive and inflexible for pHRI.

In contrast of aforementioned safeguarding devices, in our research, wearable EEG and Inertial Measurement Unit (IMU) sensors are chosen for monitoring human head motion and mental states in order to evaluate the personal safety level as well as the accident risk level. These sensors are lighter, low cost and could be integrated to any safety clothing, such as a safety helmet.

In this chapter, we present the application of IMU, especially the head-mounted IMU. And then, the algorithm of gesture recognition is reviewed. Finally, we discuss the EEG based fatigue detection.

2.1 Inertial Measurement Unit (IMU) applications

IMU sensor is a device able to measure the moving object's acceleration, velocity, orientation, using a combination of accelerometers, gyroscopes and magnetometers. With the development of semiconductor, miniature IMU with low cost and power consumption, are widely applied in motion measurement and tracking [21, 22], gait analysis [23, 24], inertial navigation and positioning [25-28] as a wearable solution, and even in robotic system using artificial intelligence [29] as an embedded component.

2.1.1 Motion measurement with accelerometer

From the kinematics, we know that the displacement of stationary object, *x(t)* could be calculated by a numerical double integration of the acceleration *a(t)*, and its noise *w(t)* with time, governed by equation (1):

$$x(t) = \iint (a(t) + w(t))dt^2 \quad (1)$$

The accelerometer is a device to directly measure the acceleration of the object. In 1999, G. Pang et al. employ a low-cost MEMS (micro electro-mechanical systems) accelerometer to measure a SCADA robot arm travelling in a short distance (40cm) and short duration [30], as shown in Fig.1.

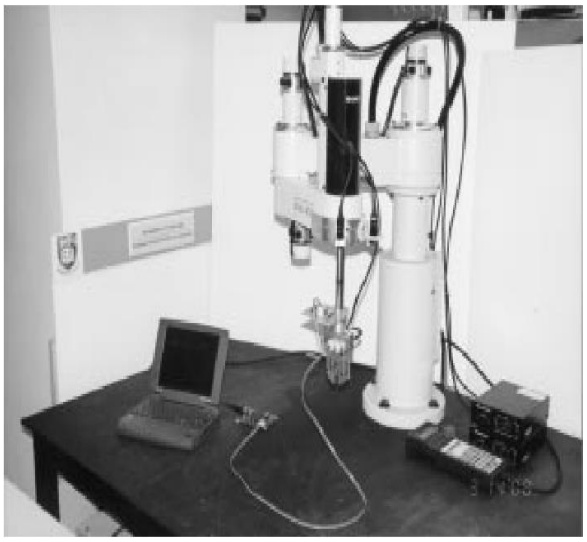

Figure 1.The prototype and robot setup [30].

Aforementioned moving tracking is uncomplicated application of IMU, since the trajectory is straight and distance is short. C. Smith et al. introduced the minimum jerk (MJ) trajectory model with acceleration input of an accelerometer-equipped "wiimote" controller to track human's arm trajectory in order to control a robot arm moving [31]. Given a starting point, an end point and a time to move between the two, the trajectory that minimizes the jerk on this interval is the MJ trajectory, where position *x(t)*, can be described as 5^{th} degree polynomials, shown in equation (2), to meet the property that the 6^{th} derivative is zero for the duration of the motion. The measured acceleration, $\ddot{x}(t)$, can be described as differentiation twice of X (t), shown in equation (3).

$$x(t) = a_1 t^5 + a_2 t^4 + a_3 t^3 + a_4 t^2 + a_5 t + a_6 \quad (2)$$

$$\ddot{x}(t) = 20a_1 t^3 + 12a_2 t^2 + 6a_3 t + 2a_4 \quad (3)$$

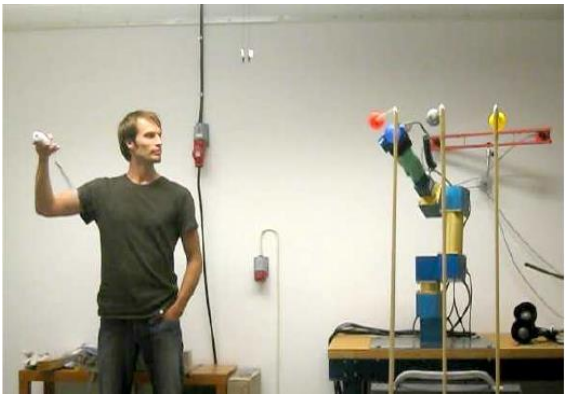

Figure 2. The real time robot arm control model [31]

The tracking method was based on the assumption that the user performed "isolated" motion, which means one motion does not start until the previous motion is ended. The velocity and position obtained from integrating the acceleration one and two times respectively was sent directly to the robot controller for real-time control to achieve simple tasks, as shown in Fig. 2. With 3DOF IMU input and using MJ model for robot trajectory planning, the author achieved real time control robot by tracking human motion, even though it cannot perform complicated continuous paths due to the limitation of tracking isolated motions of the MJ model.

Single accelerometer could be used to measure the displacement of the objects in above experiments. With complement of both gyroscope and magnetometer, the IMU sensor could measure the moving orientation of the object. Bamberg, S.J.M et al. employed a 3 DOF Gyroscope, a 3 DOF accelerometer, as well as force sensors and pressure sensors, used for gait analysis [24]. These sensors were integrated on shoes to measure the stride length, velocity, displacement by accelerometer signal integration, and measure orientation by gyroscope single integration. Figure 3 shows the Wireless Sensor System of S.J.M et al.

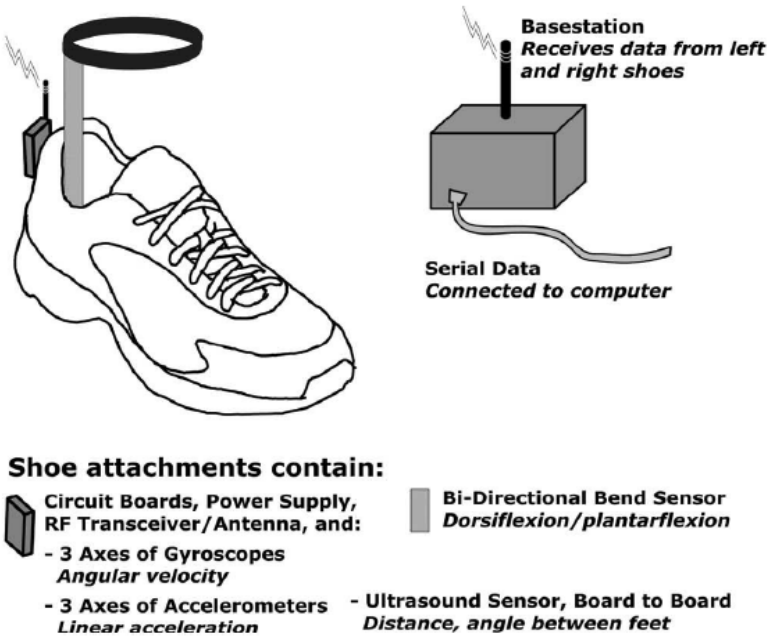

Figure 3.Shoe-Integrated Wireless Sensor System [24].

Essentially, any human motion could be divided to a series of displacements accelerated by the muscle of torso or limbs. Consequently, the body-mounted IMU is able to measure the body parts movement. The body-mounted IMU sensors are widely used in human gesture recognition. For example, Liu et al. present uWave algorithm focusing on personalized and user-dependent hand gesture recognition [32]. A single triaxial accelerometer is used to measure hand movements according to a vocabulary including eight gestures. Classification is completed using dynamic time warping (DTW) algorithm which measures similarities between two time series of accelerometer readings. Another example is found in [33], where Zhou et al. employ an accelerometer for finger gesture recognition. The time-domain analysis and forward selection algorithm of stepwise regression is adopted to evaluate finger gestures in order to get the optimal feature set. Also, a robot-assisted living system for elderly people is introduced in [34], which fuses the data collected by foot- and waist-mounted inertial sensors to recognize the subject's daily activities in order to convey control information automatically to the assisting robot.

With the development of MEMS, miniaturization of the chip size and cost reduction, the IMU sensors are widely adopted as wireless wearable solution for human tracking, gait

analysis, indoor navigation, and artificial intelligence research. Meanwhile, the measurement error caused by the IC bias, temperature, algorithm is playing an important impact for the accuracy enhancement. The algorithms are discussed in next section.

2.1.2 Error estimation and reduction for IMU signal

The MEMS sensors are small and light, but the random bias drift noise and thermal bias drift can cause the measurement error. This error could be magnified by double integration for displacement estimation. Consequently, an appropriate algorithm should be used in order to reduce the drift integration. This algorithm should be able to make a good estimate of position and orientation coming from IMU sensors measurement. Usually, a Kalman filter is introduced to make this estimation and reduce the impact of random white noise during the double numerical integration such as presented in [30].

The Kalman filter is linear estimation algorithm, actually could be called as estimator, using observed data including noise to produce optimum estimate of the system. The system may be described in a state space form [35]:

$$X_{k+1} = \emptyset_k X_k + w_k \tag{4}$$

$$Z_k = H_k X_k + v_k \tag{5}$$

where, X is called the *state vector*. It is composed of any set of variables sufficient to completely describe a dynamic system without a control-input. $\emptyset_k$ is the state transition matrix. w_k is the process noise which is assumed to be a zero mean normal distribution with covariance matrix Q_k, which is not exactly the case. Z is called the *observation vector*. It concerns data that can be known through measurements. H_k the observation matrix. v_k are measurement white noise with known covariance matrices R_k. Q_k and R_k are assumed to be mutually independent.

The Kalman filter is based on a recursive algorithm. At time t_k, the optimum combination of measured and estimated results is given by:

$$\hat{X}_k = \hat{X}_k^- + K_k \left(Z_k - H_k \hat{X}_k^-\right), \tag{6}$$

where $\hat{X}_k^-$ denotes the a priori state estimate. The 'hat' denotes an estimate and the superscript minus indicates that this is the best estimate prior to assimilating the measurement at t_k. The Kalman filter gain K_k can be written as:

$$K_k = P_k H_k^T (H_k P_k^- H_k^T + R_k)^{-1} \quad (7)$$

where the error covariance matrix P_k associated with the optimal estimate is obtained from:

$$P_k = (I - K_k H_k) P_k^- \quad (8)$$

To recursively compute the Kalman filter gain for the next step, the predictions for the state estimate and covariance at the next step are given by:

$$\hat{X}_{k+1}^- = \emptyset_k \hat{X}_k \quad (9)$$

$$P_{k+1}^- = \emptyset_k P_k \emptyset_k^T + Q_k \quad (10)$$

The Kalman filter also can be used to combine measurements from multiple sensors and provide both an estimate of the current state of a system and a prediction of the future state of the system. This algorithm is already widely implemented in navigation system, object tracking, sensors fusion, etc. to get more precise position estimation [36, 37]. Foxlin pioneered the use of Extended Kalman filter and Zero Velocity Updates (ZUPTs) to estimate the step vector from step to step with a higher accuracy to subtract the errors in the navigation states [38, 39].

2.1.3 Head- mounted IMU for human head tracking

In head-mounted display (HMD) field, Foxlin et al. presents two commercial IMU sensor systems designed for head tracking applications [40, 41]. Sensor fusion is performed by a complementary Kalman filter to weigh the gyroscopic angular rate and gravimetric tilt by accelerometer. In [42], Menz et al. use the harmonic analysis of head-mounted accelerometer signal to assist the gait pattern analysis for aging people falling risk evaluation.

In [43], A. Pajkanović, and B. Dokić use a head mounted accelerometer to control a wheelchair. The head motions are characterized in order to generate commands forward, backward, turn left and turn right. Since this system only need four commands to control the wheelchair, the head sway towards corresponding directions until exceeding the present threshold could satisfy this requirement, such as shown in Fig.4.

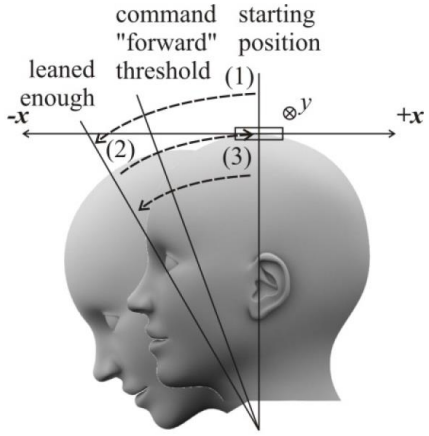

Figure 4. Generate a command – "forward" as explained in [43]

In our project, helmet-mounted IMU sensors are exploited to recognize head gesture (yes, no, look up and down) and some activities (walking, turning and climbing). These gestures and activities need to be classified using patterns recognition algorithm in order to detect the human status, further determine the human's intention and potential mental state, and then be used for risk level analysis. The next section will explain some algorithms for gesture and motion recognition.

2.2 Algorithm for Gesture and Motion Recognition

Normally, wearable sensors based motion recognition requires two stages: training and testing. In [44], Lara et al. summarize the common data flow during the two stages, illustrated in Fig. 5. At training phase, raw data is collected corresponding to each motion to training dataset. Then, the features, such statistics features in time domain, of these motions are extracted for system training.

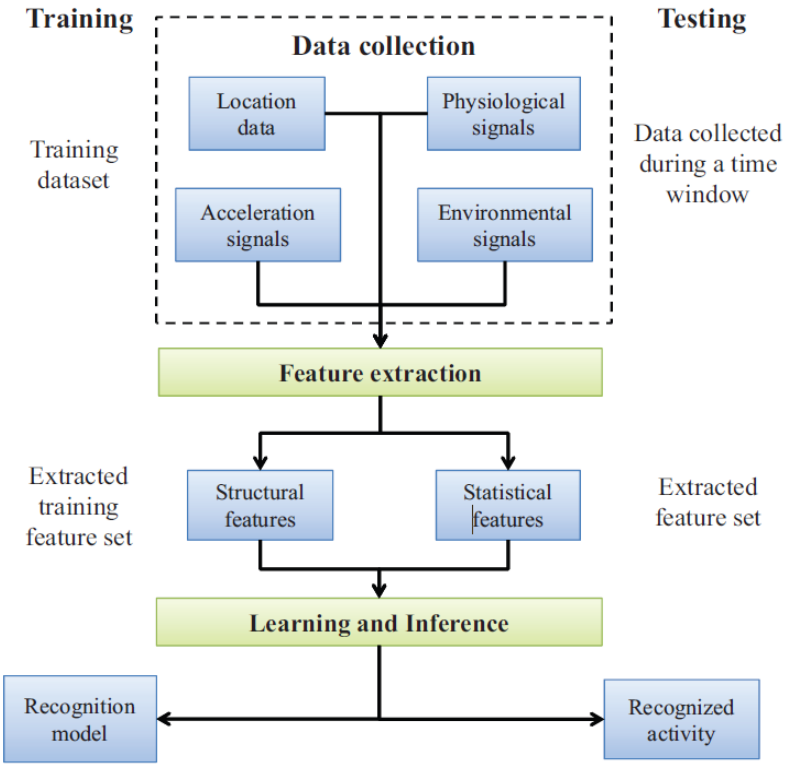

Figure 5. General data flow for training and testing motion recognition systems [44].

In the following subsections, we present some different algorithms use in this research for signal segmentation and classification. First, we present cross-correlation, and then multilayer perceptron is introduced.

2.2.1 Cross-correlation

Cross-correlation is technique which could be used to compare the spatial similarity between two vectors. The digital implementation of the cross-correlation function between two discretely sampled signals x and y is given by equation (11):

$$R_{xy}(\tau) = \frac{\frac{1}{N}\sum_{i=1}^{N}(x_i-\mu_x)(y_{i+\tau}-\mu_y)}{\sigma_x\sigma_y}, \quad (11)$$

where, $R_{xy}(\tau)$ are the cross-correlation coefficients, μ and σ and are the mean and standard deviation of the signals, N is the number of data points in the two input signals, τ is the discrete phase shift, which should be an integer [45]. The R_{xy} calculation processes involve iteratively shifting one signal forwards or backwards against the other signal that is held stationary at each increment size τ. $R_{xy}(\tau)$ should have a maximum value occurring at a

phase shift where the two signals are most similar to each other. Fig.6 shows an example of the cross-correlation calculation process. R_{xy}[n] is the cross-correlation of x[n] and y[n]. The dashed box is moved left or right so that its output points at the sample being calculated in R_{xy}[n]. The indicated samples from x[n] are calculated with corresponding samples in y[n] according to equation (11).

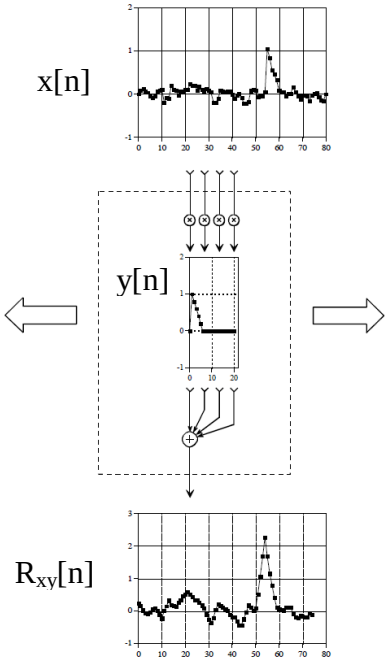

Figure 6. Flowchart of how the cross-correlation of two signals is calculated [46].

Cross-correlation has been used in many human movement studies. In [47], cross-correlation was exploited to examine the relationship between the movements of the spine and hip using an electromagnetic tracking device attaching to human body. In [48], cross-correlation was used to compare the dynamic electromyography (EMG) signals of muscle during different walking trials.

In our project, cross-correlation was used to study the similarity between predefined head motion patterns and new acquired data to identify the motion. Cross-correlation is not enough for signal analysis and classification of risk level. Then, the next section presents artificial neural network in order to improve classification of head gesture and EEG.

2.2.2 Artificial neural network: Multiplayer Perceptron

An artificial neural network (ANN) consists of a number of simple processing units, called neurons, which communicate by sending signals to each other over a large number of

weighted connections. Each unit performs a relatively simple computation: receive input from neighbours or external sources and use this to compute an output signal which is propagated to other units. The simplest ANN is single layer network with one output and two inputs, which could be called Perceptron and could be used to classify the linearly separable two classes. The input of the neuron is the weighted sum of the inputs plus the bias, and the output of the network is formed by the activation function.

The single layer perceptron only can solve the linearly separable problem. This limitation could be overcome by multilayer perceptron trained with back-propagation algorithm. A multilayer perceptron is a feed-forward neural network with one or more hidden layers. The network consists of an input layer of source neurons, at least one middle or hidden layer of computational neurons, and an output layer of computational neurons.

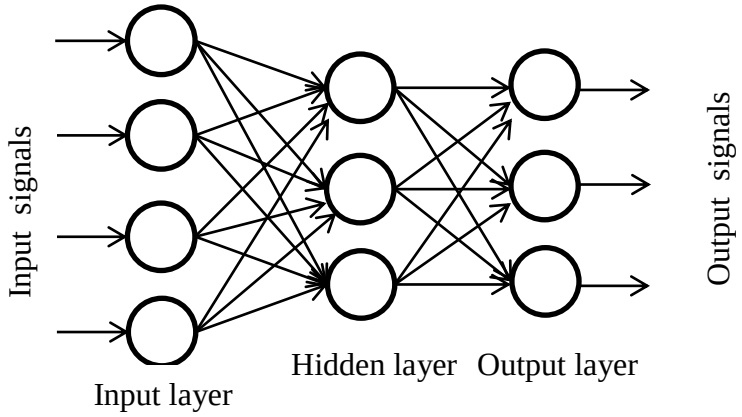

Figure 7. Multilayer perceptron with one hidden layer

Learning in a multilayer network proceeds the same way as for a perceptron. First, a training set of input patterns is presented to the network, and then the network computes its output pattern. If there is a difference between actual and desired output patterns, the weights are adjusted to reduce this error. Since the error is calculated and propagated backwards from the output layer to the input layer, this algorithm is usually called back-propagation (BP) learning.

Multilayer feed-forward network are widely used for pattern recognition. In [49], J.-S. Wang and C. Fang-Chen employed a probabilistic neural network (PNN) to recognize the handwritten digits, which are acquired by an accelerometer-based digital pen. The PNN is essentially feed-forward network with four layers and implement a statistical algorithm called kernel discriminant analysis. In [50], C. Zhu and S. Weihua implement a back-

propagation network in an online algorithm to determine if the acquired acceleration signal segmentation is a hand gesture or not, then the result is passed to recognition module to identify the gesture type.

This project intends to classify 12 types of head motions by IMU sensors, so the BP network could be an alternative solution. The information obtained by IMU will be combined with the information encoded by EEG to finally determine the human's state. Then, the next section explains how to extract fatigue from EEG signals.

2.3 EEG based fatigue detection

EEG (Electroencephalography) is the recording of electrical activity along the scalp. Based on different frequencies, EEG signals can be categorized into five specific bands: Delta (δ, below 4 Hz), Theta (θ, 4–7 Hz), Alpha (α, 8–12 Hz), Beta (β, 13–30 Hz) and Gamma (γ, above 30 Hz). Previous researches have indicated that information regarding mental states, such as vigilance, sleep, awake, could be reflected in the EEG record soon and accurately [12, 13].

2.3.1 Application based on EEG spectrum

It has been observed that a decrease in the level of vigilance could be represented by an increase in theta (θ) and alpha (α) bands activity, in contrast with a decrease in beta (β) band activity from the EEG power spectra [14-16]. In practice, monitoring theta (θ), alpha (α) and beta (β) bands activities could determine if mental state is transiting from alert to non-alert which could increase the potential risk level of accident [17]. In [15], F. Sauvet et al. use (α + θ)/β power ratio from a single EEG channel to detect low-vigilance states of pilots during real flights. They reported a 98.3% detection accuracy.

In [51], changes of the alpha (α) relative power to the entire EEG signal is used to detect the drivers drowsiness. The algorithm is based on a mean comparison test, which is completely independent of objects. As shown on Fig. 8, the alpha (α) relative power in moving window 2 is compared to a fixed reference window 1.

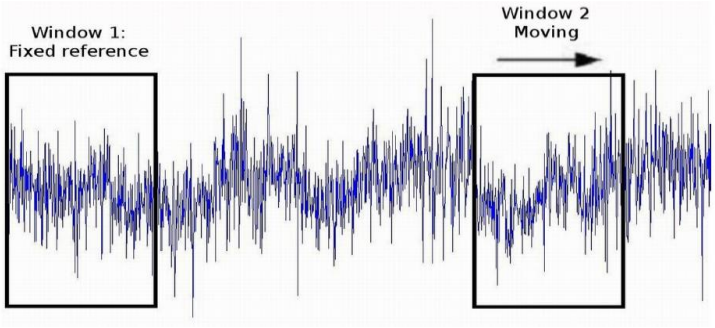

Figure 8. Illustration of windows for means comparison test in [51].

2.3.2 Eye blink extracted from EEG

Obviously, theta (θ), alpha (α) and beta (β) bands activities directly reflect the brain activities and mental states. But, the measurement of them has a high quality requirement of the contact between EEG electrodes and scalp. Fig.9-(a) shows the description of the location of scalp electrodes in the context of an EEG test. Except F_{p1} and F_{p2} (forehead), all the scalp is covered by hair, such as a sample shown in Fig.9-(b). In real time and wireless application, such as our SSH, it is difficult to make an efficient contact with those locations.

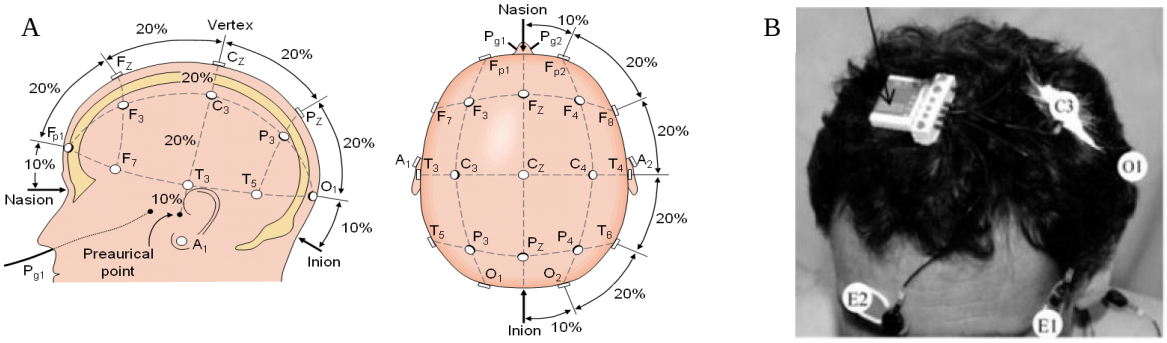

Figure 9. (a) International 10-20 system for EEG test. (b) Real two channel EEG test in [15].

During the extraction process of the θ, α and β bands, normally the first step is to remove the artefacts caused by EOG (electrooculogram), EMG (electromyography), as well as the eye blink signal which also need to be removed as artefacts noise [52, 53]. Actually, the eye blink has been proposed to be a suitable indicator for mental fatigue diagnostic [18-20]. Then it could be extracted from EEG for mental fatigue analysis since it has high amplitude comparing to normal brainwave EEG signal. For example, Fig.10 shows a typical eye blink waveform in EEG [54].

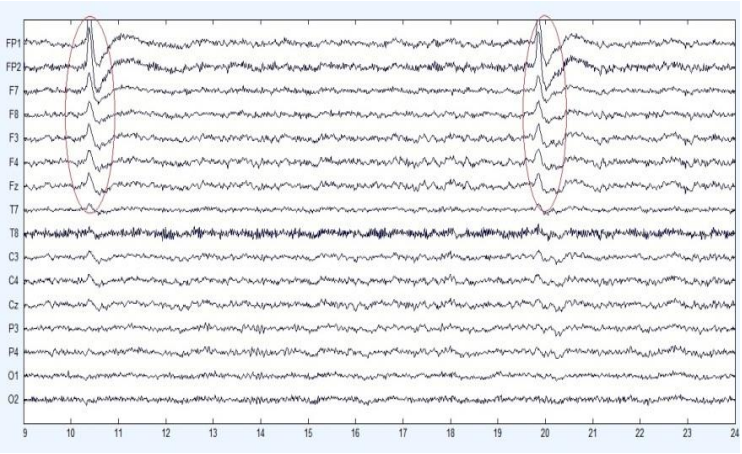

Figure 10. Typical eye blink signal in EEG [54].

Some researches with video-based eye blink detection usually employ PERCLOS (PERcentage of eye CLOSure) as the main parameter for drowsiness measurement, such as in [55, 56]. In [57], G. Li et al. estimate the eye closure degree (ECD) using EEG comparing to a video- based record. They found a linear relationship between EEG-based ECD and video-based. This means the EEG-based eye blink detection could be used to estimate the eye closure in order to detect the drowsiness and fatigue.

The blink duration and its prolongation is also found to be the most informative parameter to detect the drowsiness [20]. In [58], R. N. Roy et al. indicate that the eye blink could be characterized from frontal EEG electrodes, such as F_{p1} and $F_{p2.}$ Chambayil et al. use the kurtosis coefficient, amplitude of EEG signal to train a neural network in order to detect the eye blink event [59].

2.4 Summary

Head monunted IMU could be used to measure the head motion, and then characterize the motion in order to extract the dominant features. The algorithm of cross-correlation or artificial neural network could be used to identify the specific motion after a supervised learning. The θ, α and β brainwave bands of EEG are commonly used to estimate the mental fatigue level. As well, the eye blink also could be extracted from EEG in order to estimate the drowsiness, an indication of fatigue.

With head-mounted wearable IMU and dry EEG sensors, we can acquire the head guesture and brainwave signal wirelessly. These signals could be used to decode the human status, even the intention for personal safety level analysis in an industrial environment. In

the next chapter, we will explain our hardware and software designed for recording the human status in order to estimate the accident risk level.

Chapter 3: Suggested hardware and software

The guiding objective of this research project is to develop a device able to recognize abnormal behaviors of workers which endanger safety and health. With the development of electronic technique, a large number of miniaturized sensors could be embended into wearable devices. In an indurtrial environment, the safety helmet is a popular presonal protection equipment. So in this research, we design an inexpensive, non-intrusive and non-invasive Smart Safety Helmet (SSH) system, which is non-vision-based.

The SSH system is assembled based on a commercial safety helmet, and comprises an electronic board for real-time signal analysis, wireless transmission capabilities and three dry electrodes for EEG signal acquisition. The IMU sensors are integrated onto the electronic board, which is embedded into the specially designed safety helmet.

This chapter will first present the hardware design of the SSH system, including the helmet and electronic devices. Then, the software is explained.

3.1 Suggested hardware

The SSH system includes electronic hardware for sensing human behaviors in order to wirelessly control a machine tool. Fig. 11 illustrates the block diagram of the SSH hardware configuration: human intention measured by the IMU and EEG, wireless transmission and a receiver such as Programmable Logic Controller (PLC) able to control the industrial setup or Solid State Relay (SSR) cutting off the machine tool power supply.

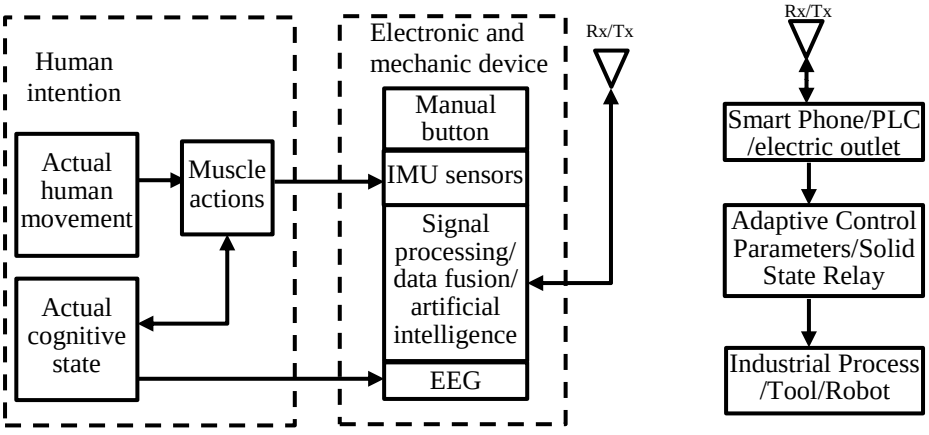

Figure 11.Block diagram of the SSH system

3.1.1 Safety Helmet.

The safety helmet is the footing of the system, which is specially designed for fixing electric board and EEG sensors. The electronic board is fixed on the top center of the helmet in order to align the vertical acceleration sensing with the center of gravity, and align the horizontal forward sensing with the sight-line. The three EEG electrodes are fixed on the front inside of the helmet in order to press against the forehead [60, 61]. Fig.12-(a) shows the coordinate frame definition of the helmet, as well as the head. The X-axis indicates forward and backward; the Y-axis indicates the left and right; the Z-axis indicated the up and down of the head. Fig.12-(b) shows the slot to hold the electric board, which is fixed on the top of the inside helmet. Fig.12-(c) shows the slots for the EEG sensors, which is installed in front of the inside helmet.

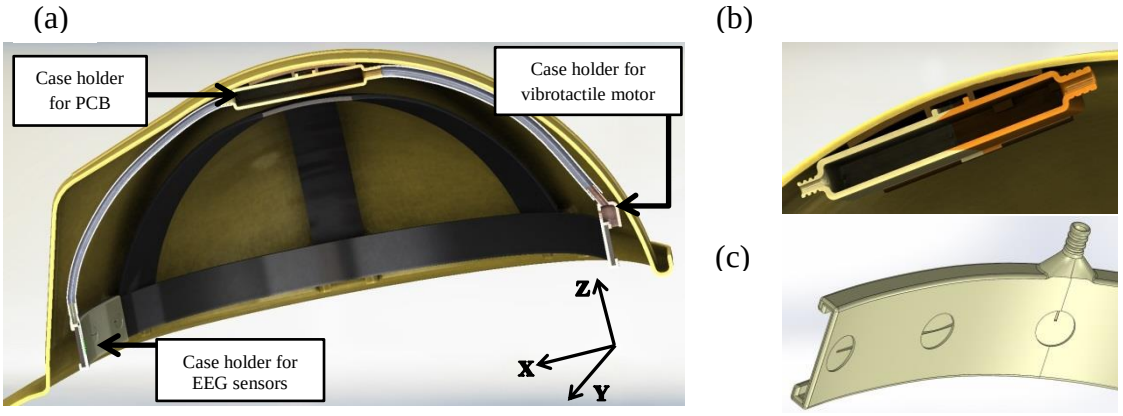

Figure 12.(a) sectional drawing of the helmet (b) electric board slot on top of the inside helmet. (c) slots for EEG sensors

3.1.2 Embedded electronic system.

The electronic device is the core unit of the Artificial Intelligence module of the SSH system, which consist of the IMU sensors for motion and gesture recognition, a PIC24 microcontroller from Microchip, a Bluetooth module for information transmission, a SD card for data record, and a USB connector for data reading and battery charge. The sensing data could be saved into the SD card or be transmitted to Android smart phone via Bluetooth module. Fig.13 shows the top side and bottom side of electric board.

The IMU sensors include digtial 3-DOF accelerometer-ADXL345, 3-DOF gyroscope-ITG3200, and 3-DOF digital compass- HMC5883L, which are connected to the same I^2C bus. In our latest version board, a sensor with high integrated level, MPU9150, is exploited.

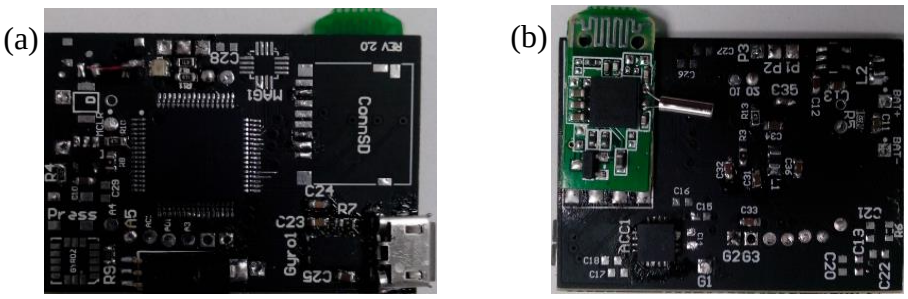

Figure 13. (a) The top side of the electronic board. (b) The bottom side of the electronic board.

3.1.3 EEG Electrodes.

The EEG is used to acquire brainwaves in order to extract mental states information. Conventional EEG electrodes used in clinic are predominately wet types with Ag/AgCl using adhesive gel interfaces. They are inconvenient to prepare and mount, especially in wearable application. The SilverBumps™ brand dry electrodes from the Orbital Company is specifically designed to be used in wearable application, as shown in Fig.14. The dry electrodes eliminate skin preparation and messy gels, which improve experience for users and easy to mount for manufacturing the helmet. The diameter of the electrode is 25 mm, and its resistance is only 0.25 Ω between surface and bottom [62].

Figure 14. (a) Side view (b) Snap side (c) Skin side of the try electrode.

The EEG electrodes are connected to the PCB board via an amplifier with 1100 gain, because the normal EEG signals are quite small, are measured from peak to peak and normally range from 0.5 to 100 μV in amplitude, which is about 100 times lower than ECG (electrocardiography) signals [63].

3.1.4 EEG amplifier.

To save development time, we buy the EEG amplifier from **Bitalino** company [64]. Actually it is designed for ECG sensor with gain at 1100 and the bandwith between 0.5-40Hz, as shown in Fig.15. Since the useful EEG frequecy for drowsiness detection are under 30Hz (β bands up limit), so it is acceptable for applying EEG signal analysis.

When acquiring the EEG signal, the electrode of IN- should be attached to the F_{p1}, and the IN+ should be clipped to the left ear, and the electrode of REF should attach to F_{p2}. F_{p1} and F_{p2} location are shown in Fig.9-(a).

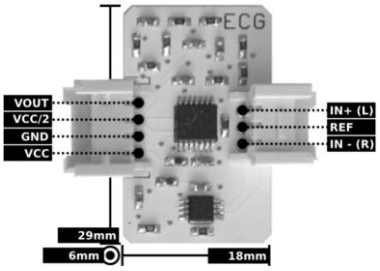

Figure 15. The ECG sensor from BITalino is used as EEG amplifer.

3.2 Suggested software

3.2.1 Firmware of Microcontroller.

Currently, the firmware of Microcontroller is inherited from IOIO [65], which is designed as interface between Android device and slave sensors. This firmwire can support the PIC24 Microcontroller to be connected to its host over USB or Bluetooth, as shown in Fig.16. There is high-level Java API on the host side for using the Microcontroller I/O functions as if they were an integral part of the client. The firmware can accept the command from Host to read sensors via I2C, SPI, UART or directly read analog input.

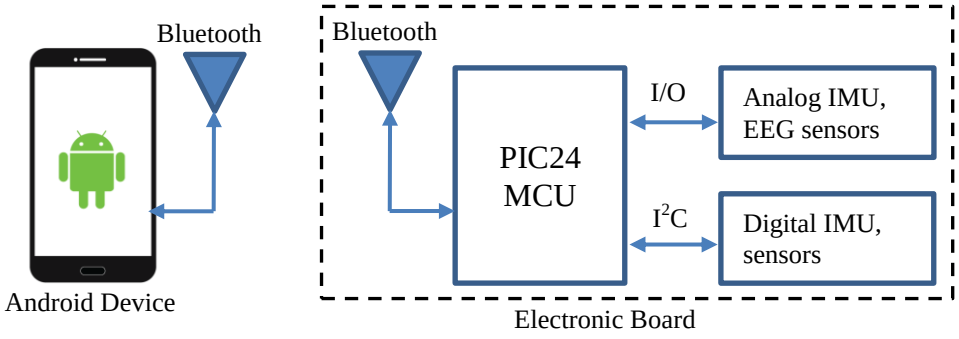

Figure 16. Block diagram of the android device to read the sensors on electronic board.

3.2.2 Application of Host side.

We developped an Android App to communicate with the Microcontroller in order to acquire IMU sensor signal. The reading could be achieved over USB or Bluetooth. This APP could display in real time the sensor result and record the data into SD card mounted on

Smart Phone at any time. Fig.17 shows the basic function of this APP to acquire the data of accelerometer ADXL345.

Figure 17. Android APP to acquire the data of ADXL345.

3.3 Summary

Our Smart Safety Helmet (SSH) is an inexpensive, non-intrusive and non-invasive wearable device system, which is non-vision-based. The high speed IMU sensors could quickly capture any head motion. Since we exploit digtal devices via I2C bus communication, the electronics are expansible or convertible to any type of digital sensors with I2C communication protocol. The dry electrodes reduce the preparation time of EEG acquisition and make it more confortable comparing to the wet electrodes with gel.

Currently, the IOIO firmware make the SSH system flexible connecting to any Andoid device for status monioring, signal acquisition, data processing, and remote control via Bluetooth. Any algorithm optimzation and feature added could be fast implemented in Java.

In the next chapter, we will talk about how to use the SSH to acquire the head motion signal and present an algorithm to identify the risky head motion in an industrial environment.

Chapter 4: Experimental research

The SSH system aims at recognizing the user head gesture and mental states in order to estimate the risk level of accident in an industrial facility. The hypothesis is then: risk level of accident could be evaluated as a function of gesture recognition and brainwaves. To achieve such purpose, it is essential to differentiate the risky head motion and mental state from the safe ones and detect situation while a worker need immediate assistance. In this chapter, we will focus on the head motions only. The brainwave part will be discussed in Chapter 6.

As discussed in previous sections, fatigue and sleepiness are considered as dangerous states for workers in industry. Usually, at the beginning of sleepiness, the head has an involuntary and sudden downward motion, named as "nodding off", and following the rotation in the Y-axis defined in Fig.12-(a). In the context of this research, identifying this type of head motion can represent the "fatigue and sleepiness state" of the worker from the view of gesture recognition.

This chapter will describe the strategy for head motion measurement. Then, a cross-correlation based model is built for head motion identification. Next, the algorithm is explained. Finally, four results, including algorithm validation, real time simulation, algorithm improvement, and application expansion, are presented and discussed.

4.1 Head motion and gesture

Essentially, any human motion can be divided into a series of acceleration and deceleration of the torso or the limbs. The body mounted accelerometer could measure in real time the body motion, and then represent the motion with acceleration features. Furthermore, the gravity also causes a static constant acceleration *G*, normally equal to $9.8 m/s^2$. Consequently, the gravity acceleration could be used the estimate two angles (pitch and roll) of body when the body is motionless.

The proposed SSH need a database of gestures, represented by the acceleration signals, in order to make a clear differentiation of acceptable motions in a workflow compared to others.

4.1.1 Head gesture vocabulary

Simulating the activities in a real working environment, the head motions could be categorized into two groups of basic actions: body stillness and moving. To clearly describe the head motions and better understanding the motion frame, a gesture dictionary including 12 basic motions is defined and created in these two groups.

The head motions at body stillness include: nodding off (head falling suddenly and fighting it), head nod or pitch for meaning of “Yes”, head shake or Yaw for meaning of “No”, looking up (Pitch-up), looking forward or neutral position as idle, and looking down (Pitch-down) as shown in Table 1. The head motions at body moving includes: go upstairs, walk straight, go downstairs, turn left, stoop down, and turn right as shown in Table 2. The two **bold** axes constitute the moving plane of corresponding head motion.

TABLE 1.THE DICTIONARY OF HEAD MOTION AT BODY STILLNESS

Motion	Plane	Gesture	Motion	Plane	Gesture
1. Nodding off			4.Looking Up		
2. "Yes" or Pitch			5. Idle	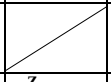	
3. "No" or Yaw			6.Looking Down		

TABLE 2.THE DICTIONARY OF HEAD MOTION AT BODY MOVING

Motion	Plane	Gesture	Motion	Plane	Gesture
7. Go Upstairs			10.Turn Left		
8.Walk Straight			11.Stoop down		
9.Go Downstairs			12.Turn Right		

4.1.2 Acceleration signal acquisition

According to the head gesture vocabulary in both Tables 1 and 2, the Smart Safety Helmet was worn to perform these actions in order to acquire the IMU signal of each gesture. A simple explanation of the vocabulary was given to the participants to understand the motions and their sequence.

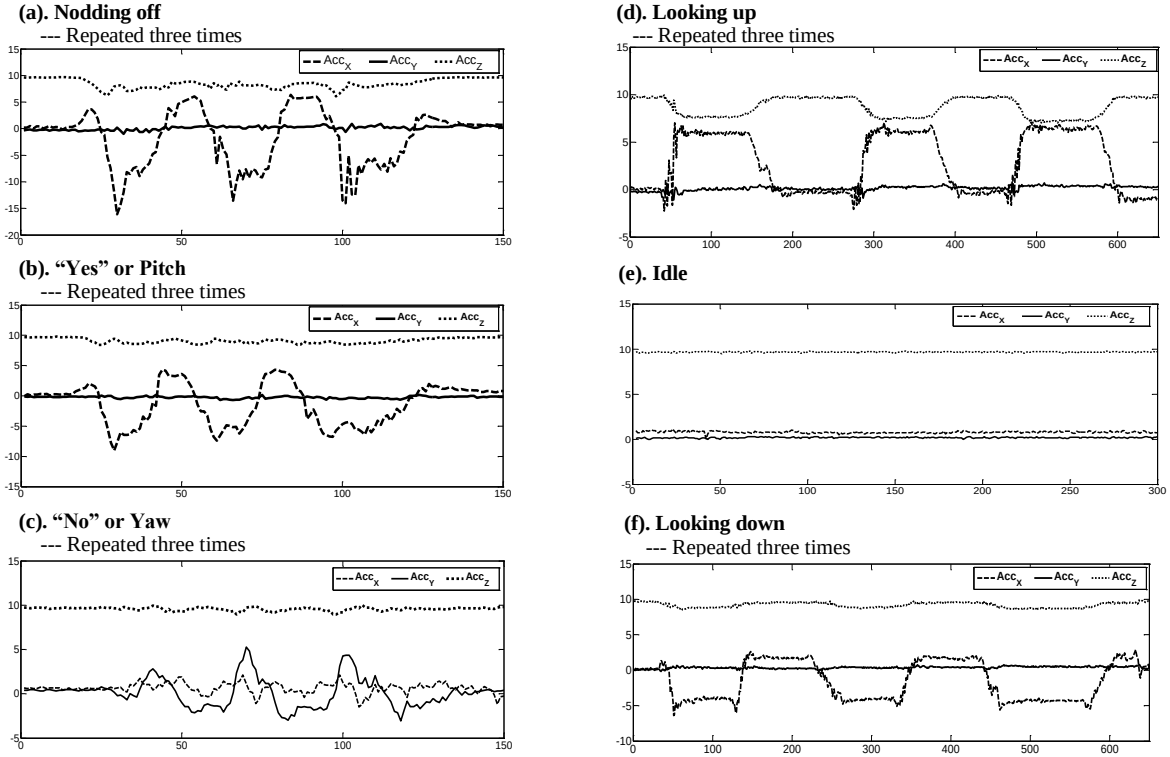

Figure 18. Triaxial acceleration signals of each head motion at torso stillness

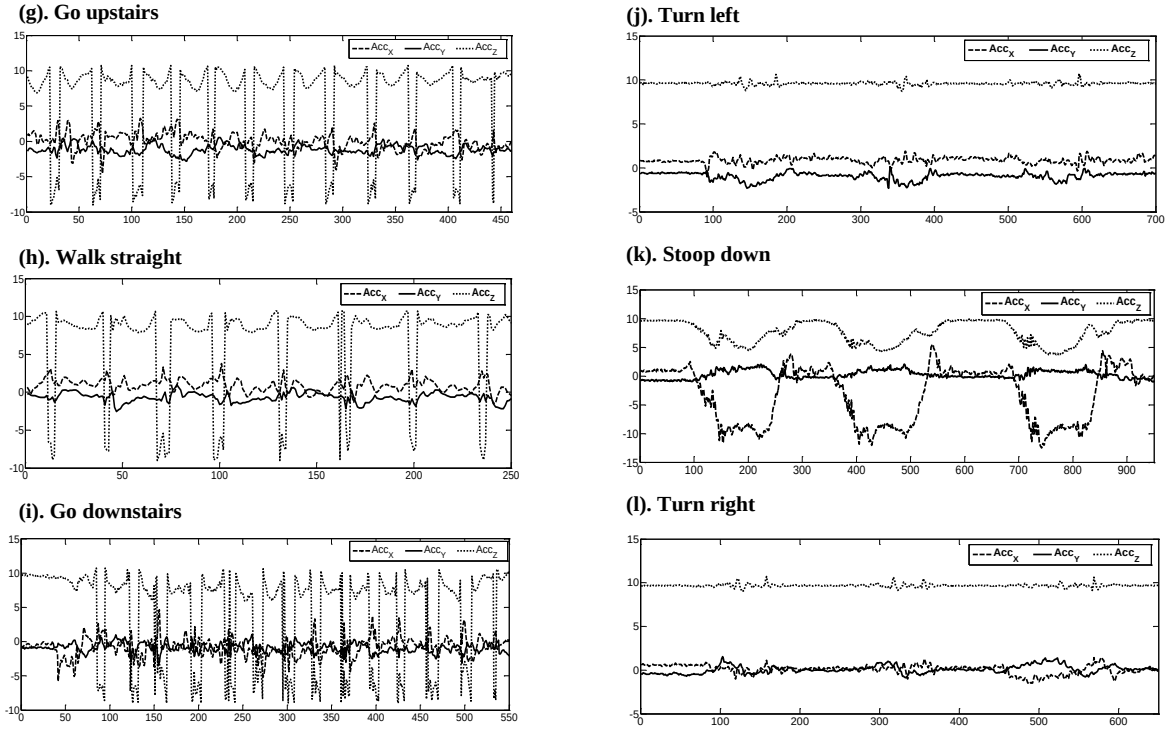

Figure 19.Triaxial acceleration signals of each head motion at torso moving

Fig.18 and Fig.19 show the first time acceleration measurement of each head motion from the same participant, as indicated by Acc_x, Acc_y, and Acc_z. These measurements were collected at a sampling frequency at 50 Hz which is enough for head motion tracking. Each motion was repeated three times per participant per gesture, except *Go upstairs*, *Walk straight*, *Go downstairs* and *Idle* where three acquisitions, approximate 2 seconds per gesture, will be used in future analysis. Fig. 18-(a) is the acceleration waveform of *Nodding off*, which could be clearly differentiated from others except (b), the waveform of *head nod* (meaning yes motion). It is because both head motions are performed by the X-Z plane up-and-down moving, as illustrated in Table 1-a / b. The intuitionistic result from these figures indicates that the acceleration signal could represent the different head motions.

4.2 Histogram of model

As mentioned in section 2.2.1, the cross-correlation algorithm could be used to compare the spatial similarity between two waveforms. The acceleration signal of predefined 12 head motions indicates obvious difference among them. In this section, we suppose that each movement is modeled statistically by a probability density estimated from the histogram. The measurement of similarity is based on the calculation of the correlation

4.2.1 Motion reference model

Since our target is to identify a motion from the predefined 12 standard motions, we have to understand the properties of them. Therefore, a motions dataset is necessary for the reference such as the y[n] defined in Fig.6, called *motion reference model*.

These 12 head motions are repeated continuously more than 20 times by the same SSH user in order to build the models. The hypothesis is that different motions include a series of acceleration values which are different from each other. Consequently, in our study, the histogram of these acceleration signals is used to represent the properties of each head motion.

The histogram analysis sorts the tri-axes acceleration signals into linear 50 bins with high limit 10 (almost equal the gravity acceleration) and low limit -10. Actually, this is a statistic model about how many data points of the acceleration signals could be sorted into each bin with 0.41 m/s^2 band. As the reference models, it is not reasonable to use quantity of data points, instead, it should use the percent to the total data points of the reference signal.

Therefore, the data normalization was adapted to build the reference models according to equation (12), where *hist* is the Matlab function to calculate and display the histogram of the data series:

$$Model = hist(a(t), bins)/length(a(t)), \quad (12)$$

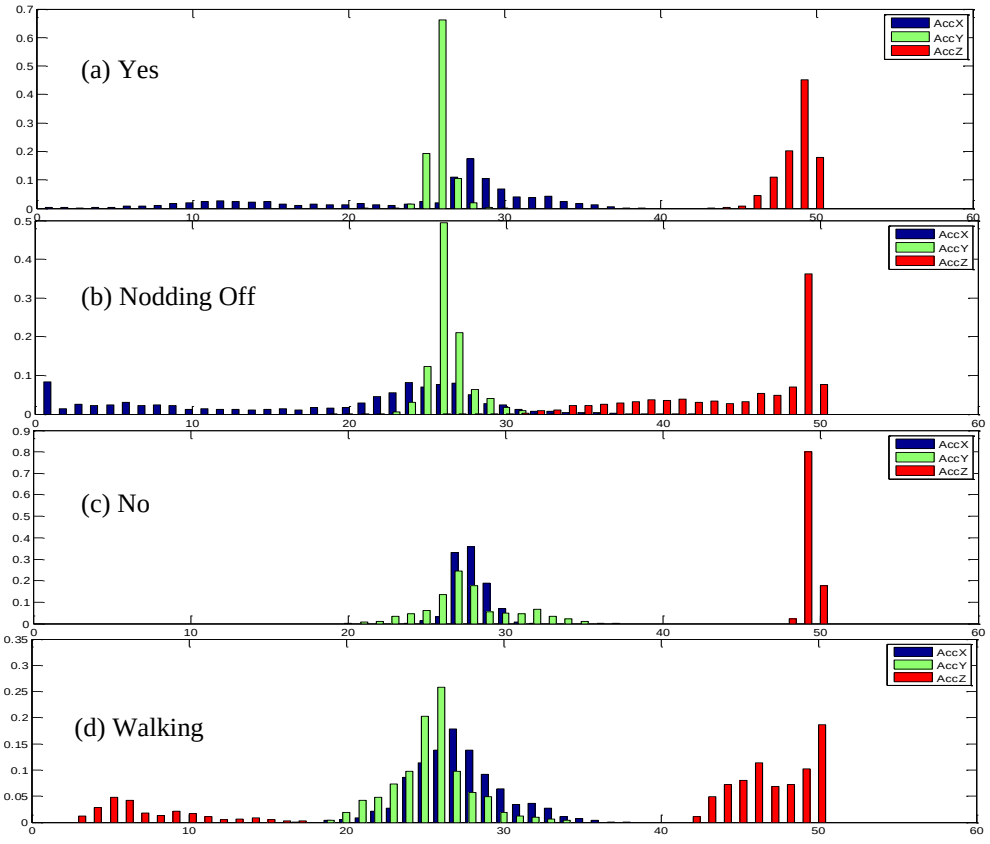

Figure 20.Normalized acceleration distribution of tri-axis

Fig.20 shows a histogram sample of motion "Yes", "Nodding off", "No", and "Walking straight" as reference models. The proportion distribution of tri-axes acceleration in each bin is represented by AccX, AccY and AccZ. The outline of different motions could distinguish each other. Even though the "Yes" and "Nodding off" are similar on the outline shape, they are obviously different on the bar distribution according to the bins detail.

All these motions reference models are used as the standard signal. The new acquired signal is the test model, which need to be compared with each reference model for identification. Before signal identification, the first step is to segment the input signal.

4.2.2 Signal segmentation for test input

The *test input* is the new acquired head motion signal used as the second input for the cross-correlation computation, such as the part of x[n] defined in Fig.6. In offline analysis, signal segmentation is necessary to locate the major acceleration values generated by the head motion events. Then, the segmented signal is compared to the aforementioned 12 head motion reference models in order to get the similarity indicated by a number between 0 and 1. The model with biggest value can be considered as the recognized head motion for the *test input* signal. In this section, we will talk about the segmentation method we used.

Essentially, each head motion consists of two steps: accelerate and decelerate, meanwhile the human head has a rotation angle limit on tri-dimensions. This means that the acceleration signal during the head motion must include "peak" or "valley" caused by the accelerating–decelerating in the motion. Fig. 21 shows the local "peak" of X-axis acceleration of "Nodding Off".

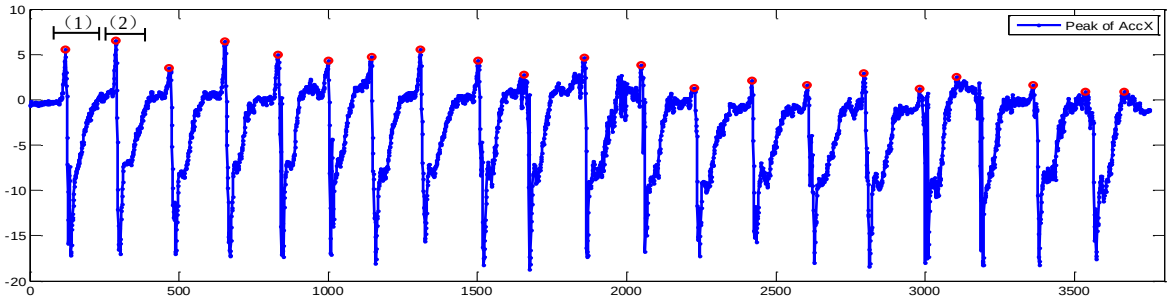

Figure 21.Peak of X-axis acceleration for "Nodding off"

For different head motions, the accelerating and decelerating features, such as magnitude and direction, are different on tri-dimensions, which generate different waveform shapes of "peak". The hypothesis is: the signal "before" and "after" a pair of peak and valley should include the information of a specific motion and could represent a head motion. Thus, in this evaluation, the signal segmentation starts with the flat signal level, a pair of peak and valley, then return to the flat level. Fig.22 shows the segment of 2 "Nodding off" samples around a local peak of X-axis, which are from the temporal windows (1) and (2) in Fig.21 with different length.

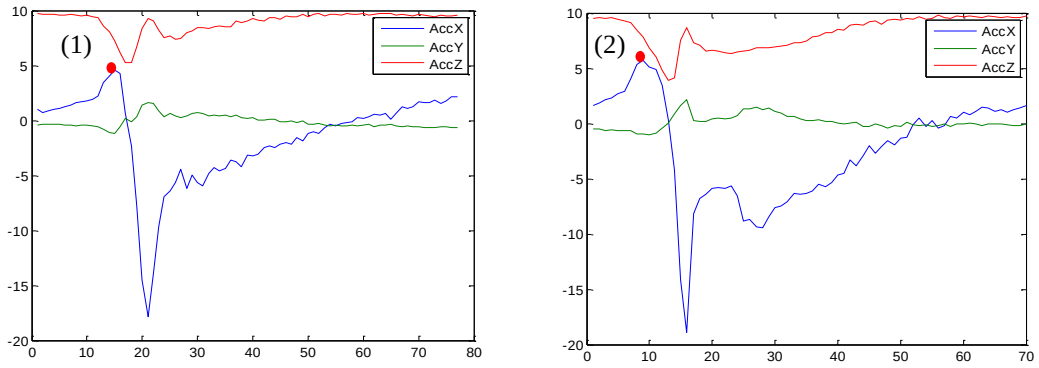

Figure 22.Segment of "Nodding Off" with different length

The segmented signal is then used to build the test input model according to the process described in section 4.2.1. The cross-correlation results between reference models and test model are used to identify the new acquired head motion signal. Fig.23 compares the test model and reference model of “Nodding off” as a sample.

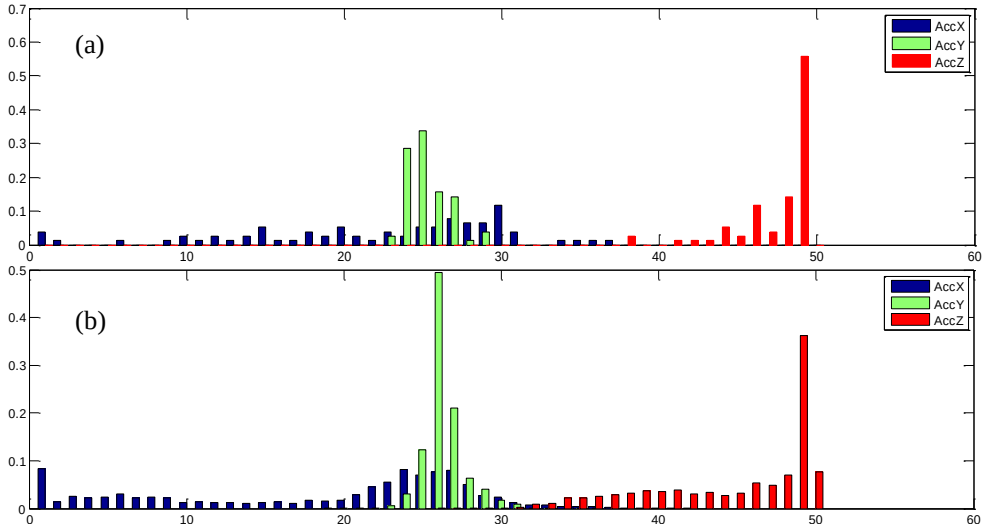

Figure 23.Nodding off: (a) test model (b) reference model

4.3 Cross-correlation computation

The cross-correlation process is based on the test model and reference model with normalized acceleration distribution of tri-axes, as shown in Fig.23. Since each model includes three axes, the computation need be executed separately according to acceleration on axis X, Y and Z. On the other hand, the acceleration of each axis is sorted into 50 bins, so the cross-correlation computation generates 99 values for each axis. Finally, each cross-correlation computation produces a 99x3 result matrix. Then, the three elements of each vector make a multiplication in order to produce the unique number representing the tri-axes cross-correlation. Fig.24-(a) shows a sample of computation results by axis, and the Fig.24-(b) is the corresponding multiplication result.

The max value of the multiplication result is used to indicate the similarity of a test model (new acquired motion data) and a reference model. Since we categorizes the head motions of 12 basic ones as shown in Table 1&2, each new acquired data, as named test model, is computed 12 times with these reference models. As a result, reference model with the max one of 12 cross-correlation values could be considered as the recognized one.

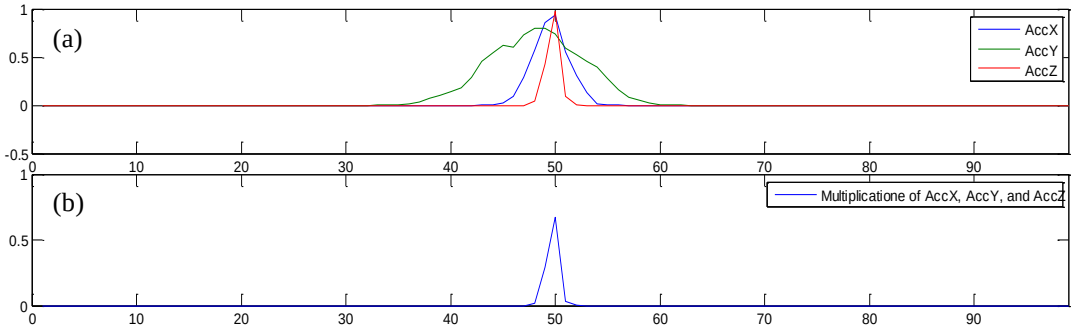

Figure 24. Cross corrolation result: (a) trend by axis (b) multiplication of tri-axes

4.4 Cross-correlation results

Four different types of data are used as the test model to present the results. First, partial data of the reference models are used in order to validate this algorithm. Then, new acquired data from the same person is used to simulate a real time computation. Next, an optimization of the algorithm is implemented. Finally, the extensive applicability of this algorithm is validated and discussed.

4.4.1 Algorithm validation

In the first step, the purpose is to validate the algorithm. Indeed the test models are built from randomly selected partial data of reference models. Then, the aforementioned algorithm was performed to verify if it works. The recognition score is 100% with training data, because all 12 test models were correctly recognized, as shown in Table 3.

TABLE 3. PARTIAL DATA OF REFERENCE AS TEST MODEL

	New captured test models											
Head motion Reference	*Nodding off*	*Yes*	*No*	*looking up*	*idle*	*looking down*	*go upstairs*	*go straight*	*go downstairs*	*turn left*	*stoop down*	*turn right*
Nodding off	0.92	0.44	0.34	0.13	0.17	0.54	0.35	0.34	0.32	0.38	0.42	0.38
Yes	0.57	0.96	0.41	0.27	0.37	0.57	0.54	0.45	0.24	0.74	0.16	0.48
No	0.31	0.37	0.93	0.37	0.53	0.32	0.35	0.25	0.27	0.54	0.09	0.85
Looking up	0.26	0.25	0.28	0.92	0.15	0.18	0.27	0.27	0.31	0.10	0.14	0.30
Idle	0.36	0.57	0.54	0.08	0.66	0.27	0.31	0.26	0.11	0.61	0.06	0.58
Looking down	0.39	0.43	0.23	0.22	0.15	0.93	0.24	0.16	0.19	0.32	0.14	0.27
Go upstairs	0.37	0.46	0.35	0.25	0.16	0.24	0.97	0.92	0.70	0.61	0.19	0.41
Go straight	0.43	0.40	0.29	0.27	0.14	0.22	0.86	0.97	0.79	0.49	0.20	0.37
Go downstairs	0.34	0.20	0.22	0.29	0.09	0.20	0.66	0.75	0.98	0.25	0.29	0.32
Turn Left	0.46	0.70	0.49	0.08	0.28	0.39	0.64	0.52	0.26	0.98	0.08	0.50
Stoop down	0.40	0.13	0.08	0.12	0.05	0.13	0.20	0.19	0.25	0.08	0.97	0.11
Turn right	0.44	0.44	0.80	0.30	0.48	0.38	0.43	0.38	0.31	0.59	0.12	0.98

4.4.2 Real time simulation

In the second step, new data was captured one more time from the same person in order to simulate the real time data acquiring. The results, as shown in Table 4, indicate that there were 4 test models were recognized incorrectly, including the "Nodding off", which is recognized as "Turn left". The recognition accuracy is 66.7% for this real time acquisition.

TABLE 4. NEW CAPTURED DATA AS TEST MODELS

	New captured test models											
Head motion Reference	*Nodding off*	*Yes*	*No*	*Looking up*	*Idle*	*looking down*	*Go upstairs*	*Go straight*	*Go downstairs*	*Turn left*	*Stoop down*	*Turn right*
Nodding off	0.41	0.27	0.28	0.08	0.35	0.12	0.31	0.10	0.22	0.05	0.28	0.38
Yes	0.39	0.53	0.30	0.06	0.50	0.18	0.26	0.32	0.24	0.16	0.16	0.22
No	0.30	0.19	0.67	0.03	0.31	0.10	0.20	0.11	0.42	0.16	0.11	0.17
Looking up	0.13	0.22	0.20	0.07	0.08	0.07	0.15	0.17	0.28	0.01	0.11	0.07
Idle	0.19	0.27	0.27	0.03	0.65	0.03	0.14	0.13	0.16	0.09	0.06	0.29
Looking down	0.35	0.24	0.20	0.04	0.13	0.13	0.18	0.28	0.15	0.02	0.09	0.11
Go upstairs	0.49	0.42	0.44	0.09	0.17	0.08	0.57	0.49	0.35	0.45	0.17	0.40
Go straight	0.50	0.40	0.37	0.11	0.16	0.09	0.51	0.37	0.50	0.33	0.16	0.43
Go downstairs	0.33	0.22	0.24	0.12	0.07	0.09	0.45	0.26	0.64	0.18	0.19	0.21
Turn Left	0.53	0.35	0.50	0.05	0.42	0.05	0.31	0.28	0.16	0.45	0.11	0.36
Stoop down	0.18	0.11	0.08	0.04	0.05	0.06	0.09	0.08	0.14	0.02	0.62	0.05
Turn right	0.34	0.31	0.50	0.06	0.35	0.10	0.22	0.11	0.48	0.11	0.11	0.44

Since we used the acceleration distribution to indicate the difference of head motions, the constant of gravity has an impact on tri-axes measurement. The tilt of head during the head motion will affect the acceleration distribution of each axis. Therefore, we need to remove the gravity in order to get a linear acceleration.

4.4.3 Algorithm improvement

To measure the real acceleration of the head, the contribution of gravity must be removed from the accelerometer data. This can be achieved by applying a high-pass filter. Conversely, a low pass filter can be used to isolate the gravity vector. Typically, an exponential moving average filter, as shown in equation (13), could be used as a low pass filter,

$$Acc\_lpf_i = \alpha * Acc\_raw_i + (1 - \alpha) * Acc\_lpf_{i-1} \quad (13)$$

where, Acc_raw_i is the raw data, and Acc_lpf_i is the low pass filtered output. α is the smoothing factor, with 0 < α < 1. Then, the linear acceleration Acc_linear_i on each axis equals

$$Acc\_linear_i = Acc\_raw_i - Acc\_lpf_i \quad (14)$$

Fig.25 is a sample of filtered acceleration signal with α=0.8.

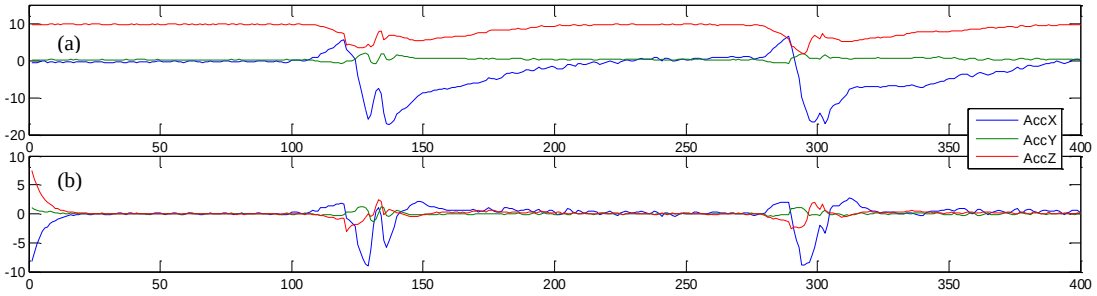

Figure 25.Application of exponential moving average filter. (a) Raw data (b) Filtered data

After implementing the high pass filter to the raw acceleration, the same cross-correlation algorithm of step II was processed, shown in Table 5. There are still 4 motions recognized wrongly, but the "Nodding off" is identified correctly.

TABLE 5. RESULT WITH HIGH PASS FILTER

	New captured test models											
Head motion Reference	*Nodding off*	*Yes*	*No*	*Looking up*	*idle*	*looking down*	*go upstairs*	*go straight*	*go downstairs*	*Turn left*	*Stoop down*	*turn right*
Nodding off	0.611	0.570	0.555	0.829	0.777	0.870	0.533	0.473	0.409	0.849	0.692	0.819
Yes	0.385	0.718	0.623	0.899	0.907	0.932	0.522	0.459	0.421	0.934	0.782	0.930
No	0.265	0.551	0.654	0.857	0.910	0.890	0.482	0.453	0.440	0.920	0.596	0.923
Looking up	0.255	0.604	0.622	0.940	0.965	0.960	0.448	0.494	0.389	0.967	0.654	0.980
Idle	0.140	0.535	0.550	0.877	0.969	0.912	0.372	0.399	0.349	0.935	0.561	0.951
Looking down	0.270	0.595	0.588	0.931	0.970	0.962	0.460	0.441	0.392	0.973	0.654	0.963
Go upstairs	0.353	0.561	0.571	0.643	0.633	0.665	0.504	0.442	0.602	0.724	0.729	0.696
Go straight	0.420	0.521	0.637	0.606	0.534	0.616	0.616	0.534	0.639	0.641	0.681	0.618
Go downstairs	0.326	0.442	0.599	0.380	0.315	0.379	0.632	0.473	0.685	0.405	0.591	0.391
Turn Left	0.197	0.579	0.603	0.918	0.981	0.941	0.425	0.448	0.389	0.971	0.620	0.975
Stoop down	0.564	0.700	0.620	0.792	0.705	0.808	0.617	0.460	0.492	0.804	0.924	0.768
Turn right	0.196	0.575	0.590	0.912	0.979	0.940	0.420	0.435	0.384	0.967	0.615	0.973

4.4.4 Application to another person

The last step is to verify if this algorithm could identify the head motions of another person based on the previous reference models. New acceleration data was captured from a different participant, and then the cross-correlation was run following aforementioned procedure.

The results, shown as in Table 6, indicate that more motions were wrongly recognized, that means it is impossible to use the reference models of single person to identify the head motions from another one. In order to identify head motions from different persons, it is necessary to collect more data of different users to build a public reference models. A magnetometer should also be used in order to increase robustness.

TABLE 6. RESULT WITH TEST MODELS OF ANOTHER PERSON

	New captured test models											
Head motion Reference	nodding off	Yes	No	looking up	idle	looking down	go upstairs	go straight	go downstairs	turn left	stoop down	turn right
Nodding off	0.738	0.564	0.830	0.835	0.781	0.900	0.331	0.356	0.140	0.793	0.765	0.852
Yes	0.530	0.522	0.895	0.931	0.861	0.959	0.250	0.320	0.120	0.910	0.737	0.861
No	0.563	0.267	0.896	0.878	0.874	0.833	0.214	0.316	0.115	0.917	0.602	0.817
Looking up	0.498	0.372	0.933	0.946	0.935	0.930	0.184	0.252	0.113	0.887	0.663	0.861
Idle	0.471	0.246	0.882	0.925	0.911	0.868	0.136	0.220	0.081	0.868	0.549	0.758
Looking down	0.487	0.408	0.943	0.976	0.904	0.948	0.183	0.262	0.112	0.891	0.686	0.849
Go upstairs	0.547	0.424	0.672	0.691	0.575	0.694	0.373	0.490	0.271	0.794	0.841	0.753
Go straight	0.610	0.403	0.617	0.585	0.540	0.615	0.468	0.520	0.325	0.696	0.810	0.758
Go downstairs	0.491	0.311	0.382	0.359	0.317	0.390	0.482	0.568	0.403	0.496	0.706	0.544
Turn Left	0.492	0.315	0.932	0.947	0.928	0.901	0.164	0.260	0.103	0.900	0.629	0.831
Stoop down	0.708	0.667	0.785	0.797	0.672	0.878	0.364	0.464	0.176	0.817	0.897	0.853
Turn right	0.494	0.313	0.925	0.951	0.921	0.904	0.161	0.254	0.099	0.899	0.625	0.822

4.5 Summary

Cross-correlation is a technic to compare spatial similarity between two waveforms. In our algorithm, each head motion is represented by discrete acceleration series. For computation standardization, these discrete series are sorted into a histogram including 50 bins and $\pm$ 10 m/s^2 limits. Then the acceleration distribution in bins is used in the cross-correlation algorithm.

The result shows that it works to identify the “Nodding off” with acceleration data preprocessing by the high pass filter, but still be confused by some actions. The reason of this confusion could come from the step that sort discrete acceleration signal into histogram, which break the temporal continuity of waveform. As a result, the different motions, which

include the same distribution of discrete acceleration signals, will have a higher similarity score.

On the other hand, it got more failures when recognizing the test models of a different person based on the same reference models. This indicates that some motions are personalised in the models used. If we want to identify head motions of different persons, we have to collect more data from different persons in order to reduce the personalized characteristics in the reference models.

In this case, we prefer to choose artificial neural network (ANN) as the further study direction because the computation time of the identification step of ANN is much shorter than the cross-correlation. And, once the offline training successes, the ANN is implemented easily in the real time application in a microcontroller. In next chapter, we will present how to implement an ANN for head motion identification.

Chapter 5: Classification by Artificial Neural Network

Artificial neural network (ANN) is a model inspired by biological neural networks and is used to imitate the functions that can learn from a large number of observed data. Artificial neural networks are generally presented as systems of interconnected "neurons" which can compute values from inputs, and are capable of classification as well as pattern recognition. For example, a multilayer perceptron (MLP) is a feedforward artificial neural network model that maps sets of input data onto a set of desired outputs using nonlinear activation function. MLP utilizes a supervised learning technique called backpropagation for training the network, and can differentiate data that are not linearly separable, such in pattern recognition application.

The supervised learning technique requests a set of training sample to train the MLP. Each example should consist of an input object and a desired output value. In this project, the desired outputs are the recognized head motion, and the input object should be the features of the desired motion. Therefore, the features must be extracted and analyzed from the raw data in order to find the appropriate ones as the input of MLP.

In this chapter, the feature extraction procedure is explained first. Then, the offline neural network training is presented. Next, the real time implementation of neural network is presented. Finally, the results are discussed.

5.1 Features extraction.

We present our algorithm in these parts in order to explain the procedure of feature extraction. The first part explains the data collection. Then, the signal segmentation is presented in order to get a time window for an analysis. The last part discusses the ANOVA results of the segment of each signal obtained from the segmentation.

5.1.1 Data collection.

According to the *head gesture vocabulary***,** 3 male students wore the Smart Safety Helmet to perform these actions in order to acquire the IMU signal of each gesture. A simple explanation of the vocabulary was given to these participants to understand the motions and their sequence. There was no special training on the vocabulary. These measurements are collected at a sampling frequency around 50 Hz which is enough for head motion tracking. Each motion was repeated three times per participant for a total of nine acquisitions per

gesture, except *Go upstairs, Walk straight, Go downstairs* and *Idle* where three acquisitions, approximately two seconds per gesture, are used in the analysis.

5.1.2 Signal segmentation.

The signal segmentation method for neural network is different from the one is used for cross-correlation algorithm presented in Chapter 4, although they are both based on the "peak" and "valley" of waveform. The cross-correlation algorithm exploits a segmentation involving a whole motion cycle, which is manually segmented. Because the segmentation is only applied to the *test model* (new acquired data), it must include all acceleration signals of a motion cycle in order to obtain accurate distribution, and then compare to the 12 *reference models*. Consequently, the length of different test models is variable.

The segmentation method for neural network is applied to both training data sets and new acquired test data. This method chooses 19 points "before" a peak and 40 points "after" the peak, for a total of 60 points in 1.2 second for features extraction of head motion. Therefore, the length of each segment is fixed counter to variable window used in cross-correlation algorithm.

5.1.3 ANOVA analysis.

Since the differentiation of the motion is target to execute on a small microcontroller, the computational burden should be limited. Therefore, using time-domain statistical feature could represent a first solution. To quantitatively identify the *Nodding off* motion from the other motions, a statistical process of all captured data is executed to compute the *mean, variance, standard deviation and signal energy*.

In order to reduce the acceleration amplitude impact (different for each participant and gesture), each segmented acceleration signal $\ddot{x}$, is normalized according to (15).

$$\ddot{x}_{nor} = (\ddot{x} - constant)/Max(|\ddot{x}|), \tag{15}$$

where, $\ddot{x}_{nor}$ is the normalized data segmentation. The constant of X-axis and Y-axis is set to zero, and the constant of Z-axis is set to 9.8 m/s^2. Then, the value of mean, variance, standard deviation and energy of $\ddot{x}_{norr}$ are computed per DOF of the IMU. Three repeated cycles of each motion were extracted for each participant, and then combined into a group. A total of nine datasets of each DOF and each motion was saved into a database for comparison. Then, an analysis of variance (one way ANOVA) were processed for the

corresponding dataset of each motion to find the most appropriate value or dataset as "indicator" to identify the nodding off motion quantitatively.

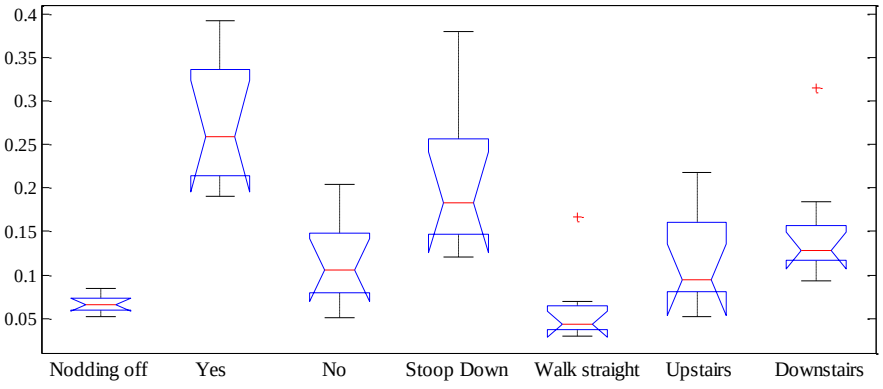

Figure 26. The normalized acceleration variance of X-axis.

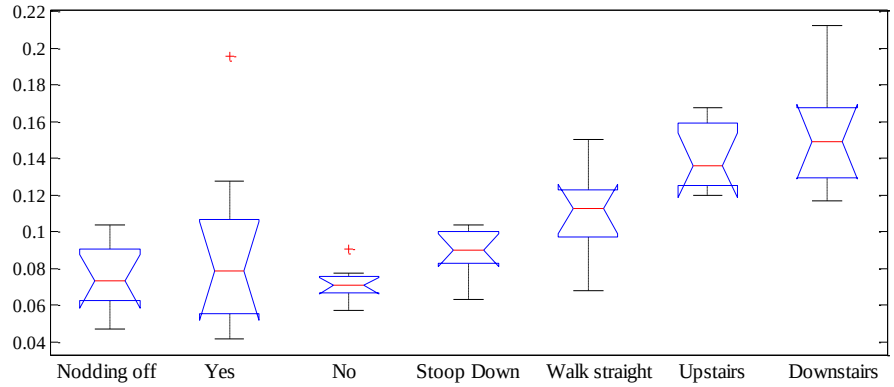

Figure 27. The normalized acceleration variance of Z-axis

Fig. 26 shows the normalized acceleration variance of X-axis with *p-value* at 4.73×10^{-10} and *F value* at 14.81. There is significant variance of acceleration in X-axis to discriminate the *Nodding off* from *Yes*, *No* and *Stoop down*. In Fig. 27, the normalized acceleration variance of Z-axis is presented with a *p-value* at 8×10^{-9} and *F value* at 12.38, which indicates that the *Nodding off* could be distinguished from the walking actions no matter straight, upstairs or downstairs. In conclusion, the acceleration variance of X-axis could be used to identify the *Nodding off* from the head motions at torso stillness, while the acceleration variance of Z-axis could be used to identify the *Nodding off* from the head motions at torso moving. Consequently, the acceleration variance of tri-axes could be used as the input of MLP.

5.2 Training the Neural Network

This section presents the offline training of neural network. The first part explains the data pre-processing. Then, the MLP configuration is explained. The last part discusses the training result.

5.2.1 Data preparation

In order to get more accurate classification, the neural network requires more training samples. According to the head gesture vocabulary, one male student wore the Smart Safety Helmet to perform these actions to acquire the tri-axial acceleration signal of each gesture. Each motion was repeated more than 20 times, and then be segmented following the method described in section 5.1.2. The mean, variance of these segments are computed.

The features of each segment was stored in a vector and then total 20 vectors of one head motion were combined into a group as the training input for neural network. The features are: 3D mean $[\overline{a_x}\ \overline{a_y}\ \overline{a_z}]^T$ and 3D variance $[\sigma_{a_x}^2\ \sigma_{a_y}^2\ \sigma_{a_z}^2]^T$. For 12 head motions, we finally have 240 input vectors for the network training.

5.2.2 MLP configuration.

A three layers MLP is created for this classification task. The input layer includes 6 neurons for the statistical feature in 3D: mean and variance$[\overline{a_x}\ \overline{a_y}\ \overline{a_z}\ \sigma_{a_x}^2\ \sigma_{a_y}^2\ \sigma_{a_z}^2]^T$. The number of neuron as an output layer equals the amount of head motion types; hence there are 12 neurons for output. To make it simple, the desired output vectors for 12 head motions are defined as a 12x12 identity matrix: each column represent a head motion.

$$\text{Desired output for 12 head motion}=\begin{bmatrix}1&0&0&0&0&0&0&0&0&0&0&0\\0&1&0&0&0&0&0&0&0&0&0&0\\0&0&1&0&0&0&0&0&0&0&0&0\\0&0&0&1&0&0&0&0&0&0&0&0\\0&0&0&0&1&0&0&0&0&0&0&0\\0&0&0&0&0&1&0&0&0&0&0&0\\0&0&0&0&0&0&1&0&0&0&0&0\\0&0&0&0&0&0&0&1&0&0&0&0\\0&0&0&0&0&0&0&0&1&0&0&0\\0&0&0&0&0&0&0&0&0&1&0&0\\0&0&0&0&0&0&0&0&0&0&1&0\\0&0&0&0&0&0&0&0&0&0&0&1\end{bmatrix}=I_{12x12}, \quad (16)$$

For the hidden layer, it seems there is no rule for the amount of neuron. There are some empirically-derived rules-of-thumb, one of these is 'the optimal size of the hidden layer is

usually between the size of the input and the size of the output layers'. In this evaluation, we tried five configurations for the hidden layer with neurons amount of 6, 8 10, 12 and 24 at different training conditions.

The activation functions for both hidden layer and output layer are the most common function used in BP algorithm, a sigmoid, since their derivatives are easy to calculate using sigmoid function and derivative:

$$f(x) = \frac{1}{1+e^{-x}}\ , \quad f'(x) = f(x)(1 - f(x)), \tag{17}$$

5.2.3 Training result discussion

The MSE (Mean Squared Error) is used to evaluate the network performance. The network training started with 6 neurons of hidden layer and 0.1 learning rate, max epoch is 100000. The neuron quantity of hidden layer increase to 24 and learning rate increases to 0.8. As a result, the best configuration appears at 0.5 learning rate and 12 neurons of hidden layer.

With the learning rate 0.5 and 12 neurons of hidden layer, we got the minimal MSE. Testing the network still got some errors, which means no input data can get an accurate matching with desired output vector in equation (16), even with the training data. Most of results are close to "1". For example, Table 7 shows the test results of the 12 input vectors of each motion, where were used as "training data" of the network. The desired output "1" varies between 0.415 and 0.992. In this case, the max value of each column approaching to "1" could be used to indicate the recognized head motion. The numbers with green text highlight mean correctly recognized, while the red one means wrongly recognized, such as vector 2.

TABLE 7. TEST RESULT SAMPLE OF 12 VECTORS FROM TRAINING DATA

Target	V1	V2	V3	V4	V5	V6	V7	V8	V9	V10	V11	V12
1	0.415	0.011	0.078	0.003	0.001	0.007	0.012	0.009	0.032	0.001	0.003	0.090
2	0.010	0.152	0.042	0.014	0.011	0.011	0.000	0.052	0.001	0.014	0.002	0.007
3	0.031	0.999	0.768	0.025	0.002	0.004	0.000	0.001	0.000	0.001	0.000	0.000
4	0.000	0.128	0.001	0.803	0.146	0.215	0.000	0.002	0.003	0.004	0.000	0.000
5	0.000	0.005	0.001	0.101	0.772	0.002	0.000	0.147	0.000	0.016	0.012	0.004
6	0.000	0.000	0.000	0.045	0.000	0.967	0.001	0.002	0.000	0.098	0.036	0.005
7	0.000	0.000	0.000	0.000	0.000	0.000	0.966	0.000	0.000	0.030	0.007	0.005
8	0.003	0.000	0.000	0.006	0.018	0.018	0.003	0.691	0.035	0.011	0.028	0.006
9	0.036	0.001	0.002	0.027	0.003	0.210	0.042	0.000	0.900	0.000	0.000	0.000
10	0.000	0.240	0.005	0.089	0.001	0.002	0.007	0.010	0.000	0.895	0.000	0.000
11	0.000	0.000	0.000	0.001	0.069	0.004	0.000	0.001	0.006	0.000	0.919	0.015
12	0.002	0.000	0.001	0.000	0.000	0.000	0.003	0.000	0.000	0.000	0.123	0.992

In another hand, the confusion matrix is used to evaluate the training results mismatch, as shown in Fig. 28. The overall training result got 90.8% matched. The “Target Class” is the desire output, while the “Output Class” is the actual output. In our result, the “Target Class 2” vectors are all mismatched to Class 1 and Class 2. Class 2 here is the motion of “Go straight”, and Class 1 and Class 3 are “Go downstairs” and “Go upstairs”.

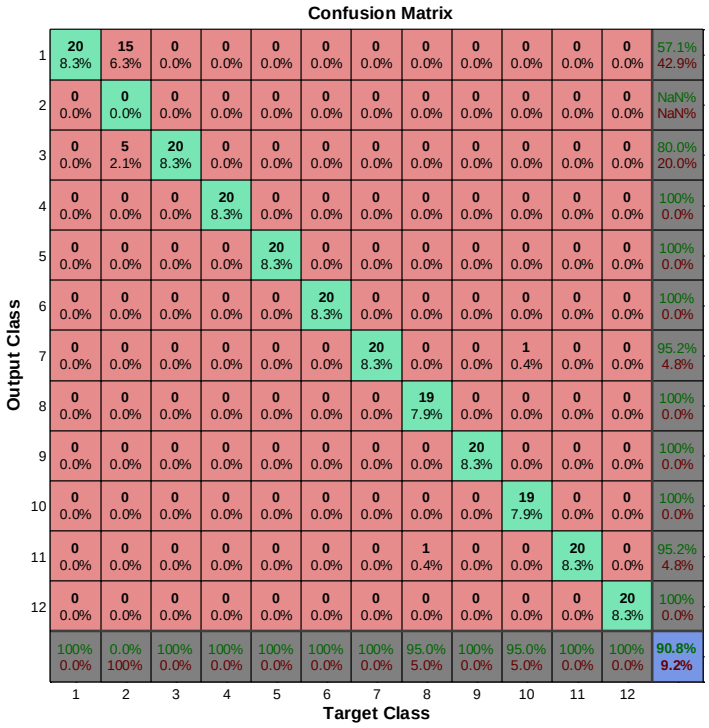

Figure 28. Confusion Matrix of the MLP training

The reason of this confusion is caused by the segmentation with fixed data points. The information included in the segment of walking depends on the walking speed. Some segments include 1 cycle, while others include more, such as shown in Fig. 29. Therefore, accurate segmentation is very important for the neural network training as well as the more training data. Indeed, a future work will consist to improve the segmentation algorithm.

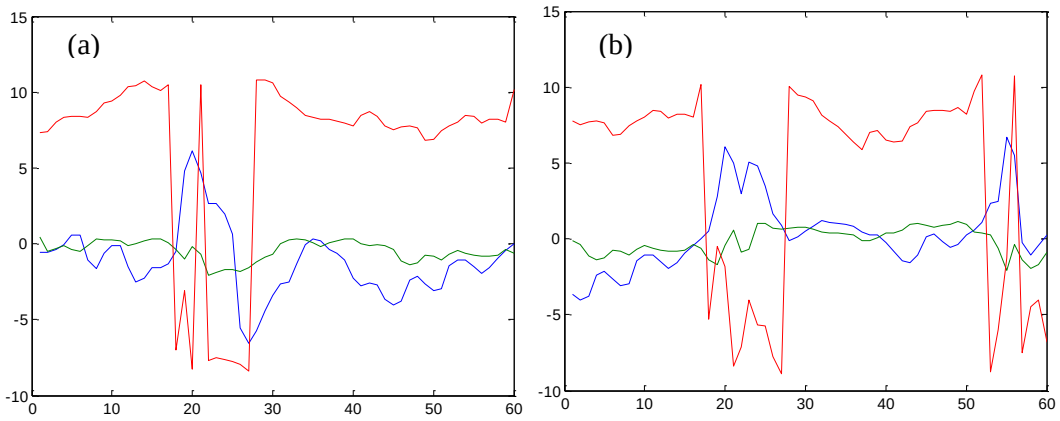

Figure 29. Segment include (a) 1 cycle (b) 1 and half cycles

In our research, we did not suppose that the "walking" is dangerous factor in an industrial facility, because a "walking" worker means he does not show a sign of "fatigue" or "drowsiness". In this case, the "walking" could be considered as a normal status during HRI. In the following section, we will remove the three head motions during "walking" for a real time implementation of neural network, and then try to improve the recognition rate of the dangerous situation.

5.3 Real time ANN implementation I

In previous research, the Helmet-mounted accelerometer is exploited to record the head gestures (yes, no, look up and down) and some activities (nodding off, walking, turning and stairs climbing). The offline analysis indicates that the normalized acceleration variance of X-axis and Z-axis could be adopted as indexes to differentiate the risky motion from others.

In this section, the Artificial Neural Network is implemented in the SSH to recognize head motions in real time, then remote control a SSR relay (explained in Appendix B) to turn off a machine- tool when a risk level increase over a threshold value.

5.3.1 Real time ANN framework

A multilayer perceptron (MLP) are trained and tested in Matlab with acceleration signal samples. Since we already acquired data of 12 head motions and we don't need the data of climbing and walking activities, so we just use 8 head motions, including "yes, no, look up and down, turn left and right, nodding off, idle" to train the neural network in order to determine the framework of the MLP. The framework will be used to configure a Java library in order to implement a real time solution for the MLP.

Based on the evaluation result in section 5.2, the final MLP framework is: 6 input neurons→12 hidden neurons→ 8 output neurons. The activation functions for both hidden layer and output layer are the most common function used in BP algorithm, which is a sigmoid function.

5.3.2 Java library for MLP implementation

In this evaluation, an IOIO is used to acquire the acceleration data, which could be considered as an interface between the IMU sensors and Android smart devices. In previous study, we already developed the code to read the digital accelerometer ADXL345. Based on this, we need develop the Artificial Neural Network in Java to run on Android device. Meanwhile, the real time signals also need to be processed in order to feed in the MLP.

To save the programming time, the online MLP involves the Encog library. Encog is an advanced machine learning framework that supports a variety of advanced algorithms, such as Support Vector Machines, Artificial Neural Networks, Genetic Programming, Bayesian Networks, Hidden Markov Models, Genetic Programming and Genetic Algorithms [66]. In our evaluation, the prepared data and network framework from Section 5.3.1 was feed in to the Java workbench, and then we got a visible network structure, shown in Fig.30. The workbench of Encog also can be used to train the network. Training the network with the acceleration data, we can get the trained weights which could be directly used in the real time MLP implementation.

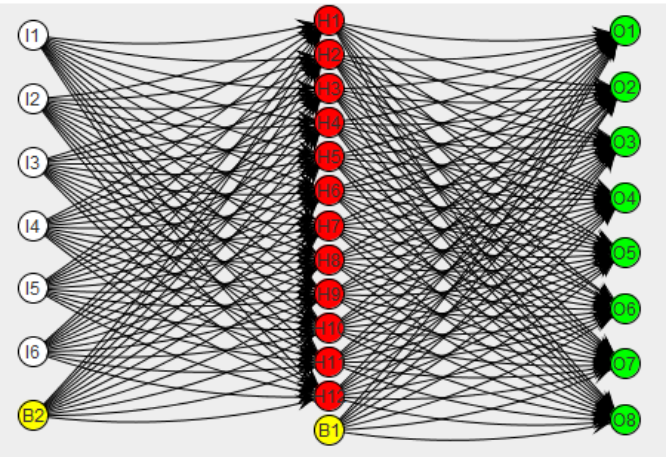

Figure 30. The MLP structure of Encog

5.3.3 Real time signal analysis

As the input of the MLP, mean and variance values are computed in the segmented signal of the pre-processed acceleration. In Java, a class named “Statistics” is developed to compute the mean, variance, max value, min value and acceleration normalization.

As the initial evaluation, we did not try to find the peak value of each signal to locate the motion transition. From the beginning of the process, a sliding window of 60 data points is used to compute the mean and variance. Then the vector is feed to the MLP to compute the output vector, including 8 elements. The biggest output value is considered to indicate the head motion.

5.3.4 Result discussion

The real time MLP algorithm was implemented in the helmet with IOIO+ Encog library. The old data was used to train the network to identify "Yes" "No" "turn left" "turn right" "looking up" "looking down" "idle" and "Nodding off". The initial result is not very accurate when it identify the "turn left" "turn right" from "No", or identify the "looking up" "looking down" from "Yes". As well, sometimes it also confused by the “Yes” and “Nodding off”.

We need reduce the motions category and combine “looking up/down/left/right” and “turn left/right” to a single category “looking away”. Then recollect more data to train the ANN to just identify the “idle”, “looking away” and “nodding off”. We hope this will increase the accuracy of head motion recognition.

As well, since we used the mean value of each axis acceleration data, the tilt of head at performing the motion will cause a projection of the acceleration vector. Consequently, we should consider correcting the rotation of head to improve the motion recognition accuracy.

5.4 Real time MLP implementation II

In this section, we reduced the motions category and combine “looking up/down/left/right” and “turn left/right” to a single category “looking away”. New data was collected to train the MLP to just identify the “idle” “looking away” and “nodding off”. This should increase the accuracy of head motion recognition. As well, a magnetometer was exploited to measure the user’s orientation, and is used in the MLP training.

A multilayer perceptron with new structure are trained and tested in Matlab with acceleration signal samples and Magnetometer signal. New data was collected at 40Hz for 3 head motions “Idle”, “look away” and “Nodding off”. These data was used to train the neural network in order to recognize the head motion in real time.

5.4.1 Magnetometer for evaluating the impact of head orientation

Since we plan to remind the user when he is “looking away” and stop the reminder when the user recovers to a normal state (idle), the initial orientation of the user must be considered to determine if he is at a correct orientation. In this trial, the magnetometer is exploited to sense the “correct” orientation and used to train the MLP. Fig.31 shows the sample of acceleration and magnetization signal for “Nodding off”.

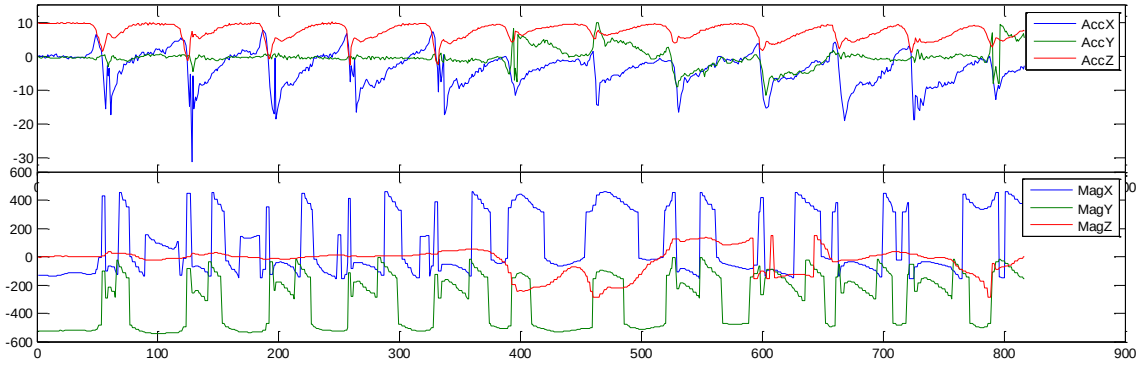

Figure 31. The Acceleration and Magnetization sample for Nodding off

Due to the limitation of communication speed between IOIO and Android device, the data reading speed is declined from 60 Hz (reading accelerometer only) to 40 Hz (reading both accelerometer and magnetometer). The measurement frequency is still acceptable for head tracking.

5.4.2 Data recollection

The new data for training set was collected at my desk when I was facing the wall in my front, so the initial orientation is “face to the wall”.

In order to improve the tolerance of the head motion variance, the “idle” state actually is not stationary. Instead, it includes a small sway front and back, right and left, around. For

the “looking away”, it includes turn and keep looking at “right, left, up and down”. The “Nodding off” is same as previously defined, fall asleep and fighting it.

The “Idle” state was collected in 90 seconds, and the “looking away” was performed in 82 seconds. The “Nodding off” data included 30 cycles in 48 seconds.

5.4.3 MLP frame determination

The new collected signals were segmented per 40 data point (1 second), including 3DOF acceleration and 3DOF magnetometer. Then, the dataset was put into a Low Pass filter to smooth the curve. Finally, the filtered dataset was used to compute a statistical feature vector including 3D mean and variance of acceleration and 3D mean of magnetization: $[\bar{a_x}\ \bar{a_y}\ \bar{a_z}\ \sigma_{a_x}^2\ \sigma_{a_y}^2\ \sigma_{a_z}^2\ \overline{M_x}\ \overline{M_y}\ \overline{M_z}]^T$. A three layers perceptron is created for this classification task. The input layer includes 9 neurons for the statistical feature. The neuron amount of output layer equals the amount of head motion types: “Idle”, “look away”, and “Nodding off”. To make it simple, the desired output vectors for 3 head motions are defined as a 3x3 matrix: each column represents a head motion.

$$\text{Desired output for 8 head motion}=\begin{bmatrix}1 & 0 & 0\\ 0 & 1 & 0\\ 0 & 0 & 1\end{bmatrix}=I_{3\times3} \tag{18}$$

The hidden layer still keeps 12 neurons.

5.4.4: Online algorithm

The Encog is still used for MLP programming. As the offline MLP descripted in last section, the online MLP comprises the same frame: 9 input neurons, 12 hidden neurons, and 3 output neurons. The input data of MLP includes 3D mean values of acceleration, 3D variance of acceleration, and 3D mean value of magnetization. Before input to the MLP, the acceleration and magnetization is filtered by a low pass filter. The procedure of this algorithm is shown in Fig.32.

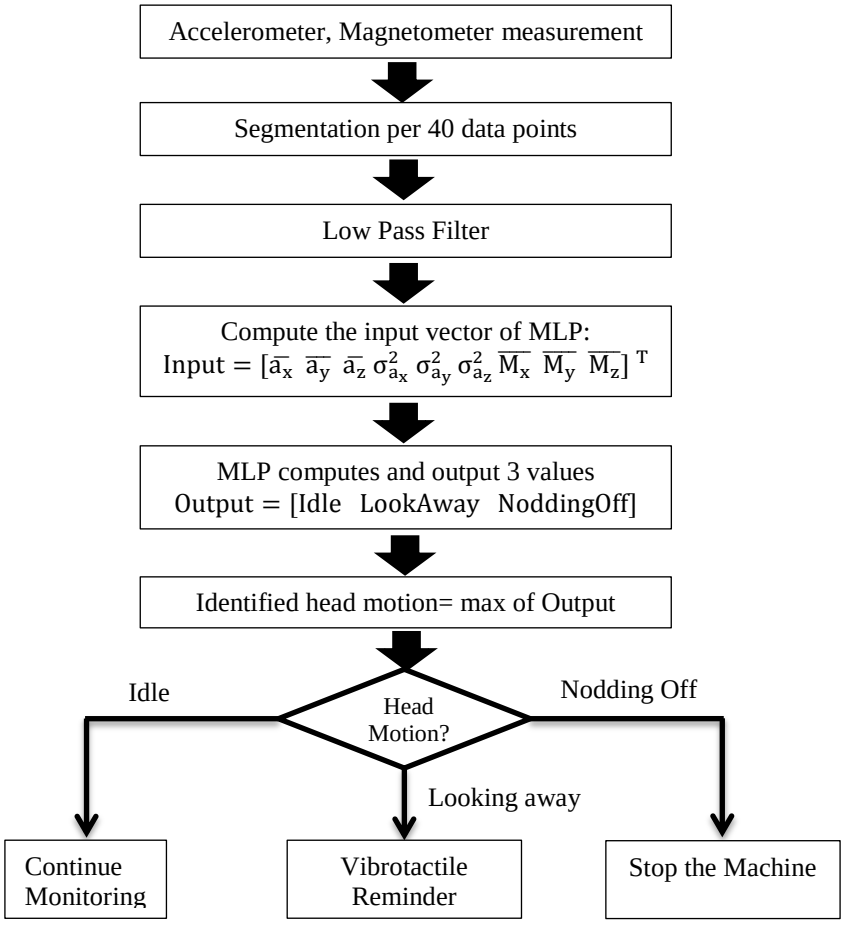

Figure 32. Real time algorithm for head motion recognition

5.4.5 Online head motion recognition result

With the algorithm, as shown in Fig.32, and trained by personal data, an online experiment was performed. The three status head motions were performed several times respectively by one person. The recognition accuracy could achieve over 85%, as shown in Table 8.

TABLE 8. ONLINE HEAD MOTION RECOGNITION RESULT

Input Motion	Performed Times	Recognized as			Accuracy
		Idle	Look Away	Nodding Off	
Idle	28	24	4	0	85.7%
Look Away	31	2	28	1	90.3%
Nodding Off	29	0	3	26	89.6%

5.5 Summary

The real time ANN algorithm was implemented in the helmet with IOIO+Encog library. With the “Max output” algorithm for head motion identification, the accuracy could achieve over 85% for single person validation in trial II. With the magnetometer, we define the correct initial orientation, which successfully identify the “look away”, and do not depend on the specific head motion or posture. Meanwhile, the magnetometer also limit the real application condition, that means if we get the training data of one specific orientation, we have to perform the online experiment following the same orientation.

In a real working environment, this should not be a problem because the location of the machine should be fixed and the normal orientation of worker should be known. In the future work, we could implement a Fuzzy logic instead of “Max value” only, and we could consider the previous identification result and the later one. As well, clearly boundary definition of “looking away”,” idle” and “Nodding off” could help to reduce the noise during the data acquisition, which could help to improve the accuracy and robustness.

Fatigue detection by head motion is not enough to estimate the accident risk level. Mental state is another approach to detect fatigue. In the next chapter, we will explain how to estimate the vigilance level by eye blinking extracted from EEG signal.

Chapter 6: EEG signal analysis

Some mental states, such as fatigue, drowsy or sleepiness are known to increase the potential of accidents not only in industry when using a machine tool, but also in vehicle driving. The highest rate of industrial accidents is usually found among shift workers due to fatigue or extended work hours [10]. For vehicle drivers, it is estimated that about 20% of fatal collisions involve driver fatigue, calculated by eliminating other possible causes such as alcohol impairment, speeding, unsafe passing, etc. [67]. Mental fatigue can increase the potential of personal injury and death, but it is complex to measure and quantify. Usually, the fatigue can cause yawning, eye blink slowly even close, or head nodding off. Previous sections mainly focus on the head nodding off detection caused by the drowsiness. This section focuses on the mental fatigue which is measured by EEG.

EEG is the recording of electrical activity of the brain. Previous researches have indicated that information regarding mental states, such as vigilance, sleep, awake, could be reflected in the EEG record soon and accurately [12, 13]. It has been observed that a decrease in the level of vigilance could be represented by an increase in theta (θ) and alpha (α) bands activity, in contrast with a decrease in beta (β) band activity from the EEG power spectra [14-17] . Consequently, many researches are inclined to exact the θ, α, and β frequencies of EEG in order to analyse the mental fatigue, such as presented in [15, 51].

As mentioned in previous section, most of the scalp is covered by hair, which is an important issue of contact between EEG electrodes and skin. Each region of the brain had a characteristic alpha rhythm, but alpha waves of the greatest amplitude are recorded from the posterior regions of the cerebral cortex. As a wearable device, the SSH integrates the EEG electrodes in the forepart in order to contact with forehead, where has thinning hair. This area is close to the eyes, so the EEG is affected by eye blinking and eye movement (electrooculogram). Actually, the eye blink has been proposed to be a suitable indicator for mental fatigue diagnostic [18-20]. Indeed it could be extracted from EEG for mental fatigue analysis since it has high amplitude comparing to normal brain EEG signal.

In our research, eye blink is extracted from EEG which is measured from forehead. The next section explains the signal while the other sections explain a method in order to evaluate fatigue.

6.1 EEG measurement

The EEG signal is measured at 100Hz. The eye blink has obvious higher amplitude than other rhythms, as shown in Fig.33, which is a record of 80 seconds. On this figure, the signal is characterized by:

1. The spikes in green rectangle are the normal blink.
2. The spikes in red rectangle are the fast blink.
3. The spikes in red round are caused by eye open.
4. The waves in black rectangle are caused by eye close.

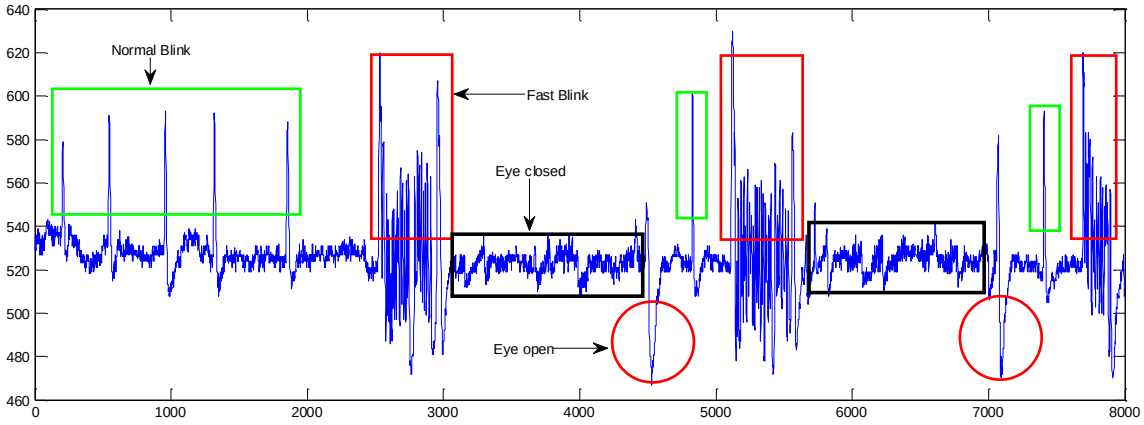

Figure 33. EEG signal samples measured by SSH

6.1.1 FFT of the sample signal

The FFT analysis of above record indicates that the major power is from the frequencies less than 3 Hz, which is the eye blink frequency. The energy between 7-8Hz (theta to alpha rhythm) probably is caused by longer time eye-close in black box.

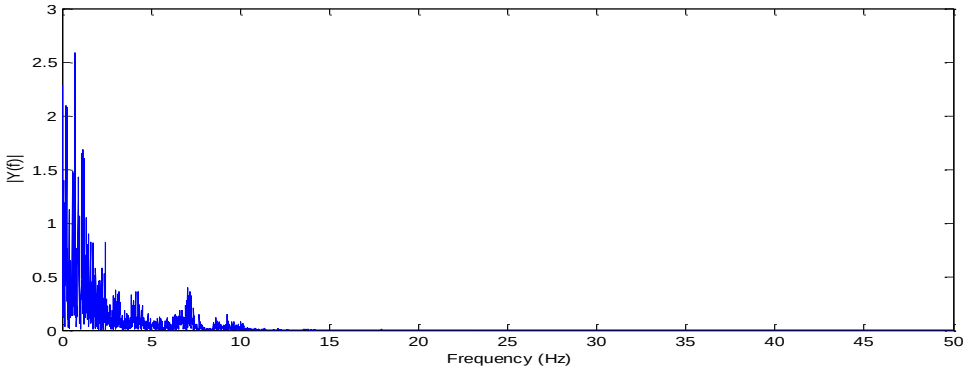

Figure 34. FFT of the EEG samples.

6.1.2 FFT of eye-open and eye-close

Since the frequency of Theta (θ, 4–7 Hz), Alpha (α, 8–12 Hz), Beta (β, 13–30 Hz) could be used to estimate the vigilance level, a band pass filter is applied to screen them out from the sample signal. After manually removing the eye-blink, the signal during eye-open and eye-close is analyzed separately, as shown in Fig. 35.

The FFT result shows that the β band, marked by green and red rectangle, decreases during eye close, while the θ and α band increase. The power ratio of (α + θ)/β can be used to estimate the vigilance level as well as the fatigue. The bigger ratio indicates a higher fatigue and lower vigilance.

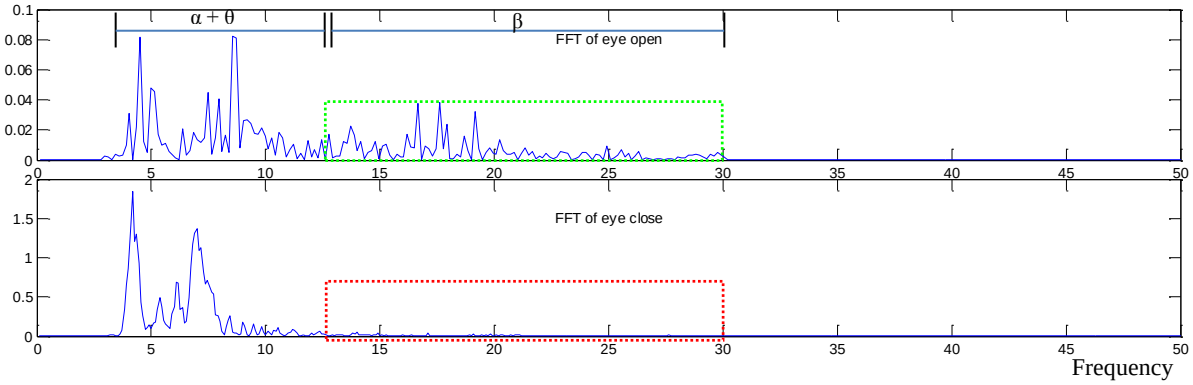

Figure 35. FFT of eye-open and eye-close EEG samples.

6.2 Eye blink detection

Even though the eye blink signal has higher amplitude, we cannot directly exploit the absolute value to detect the blink. Because the contact issue of EEG electrodes may cause an unstable measurement, which introduces different artefacts. Therefore, an indicator of eye blink should be extracted for offline and real time implementation. The first step is applying a filter to remove the constant and noise using a band pass filter.

6.2.1 Band pass filter

In order to detect the eye blink from EEG signal, we applied a band pass filter with 1-3Hz to remove the constant (0 Hz) and noise. Other band pass filters could be designed in order to extract each sub-band for brainwaves analysis (for example: Alpha, Beta and Gemma waves) in the future.

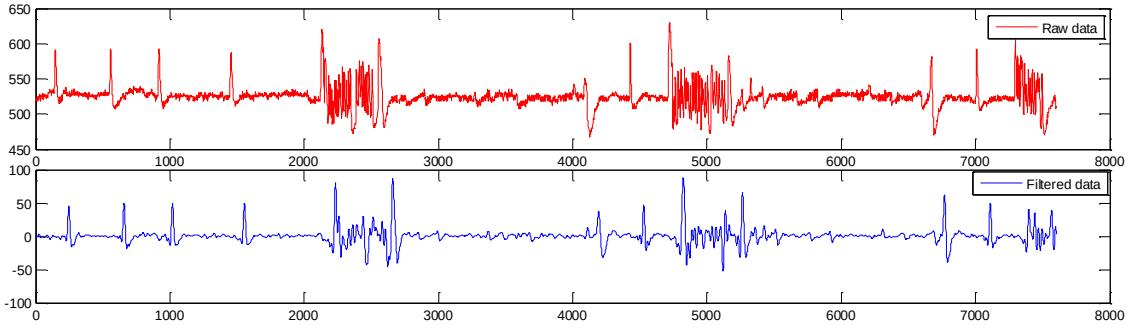

Figure 36. Band pass filting of EEG signal

6.2.2 Kurtosis and Variance

Based on the filtered data, the Kurtosis and variance is computed in order to find the indicator for the eye blink. Both statistics values are calculated per 50 points using an overlap of 49 points with a sliding window. This algorithm intends to find the trend of statistic features by observation of temporal values.

As illustrated in Fig.37, the variance of the signal is more obvious to indicate an eye blink event in the filtered EEG signal. On this figure, Δt1 is the blink duration, and Δt2 is the blink interval. In the real time application, this could be an option for blink detection. As well, combining the peak of filtered EEG and its corresponding variance could increase the accuracy of blink detection.

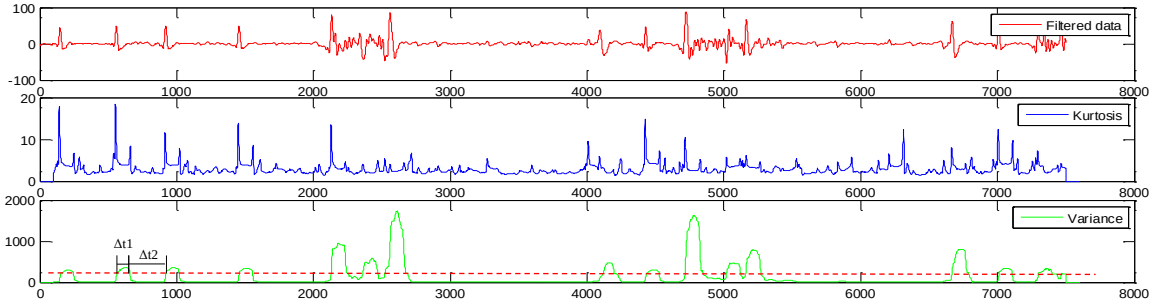

Figure 37. Kurtosis and variance of filtered EEG signal

6.3 Algorithm of fatigue detection by eye blink

Once a blink is detected, the duration of it should be measured in order to determine if the user begins drowsiness. The normal spontaneous blink duration (BD) is between 300ms and 400ms. The closure excessing over 1000ms is recognized as microsleep. The blink duration and blink rate are widely used to detect the driver fatigue [68, 69].

In this project, the normal blink duration up limit is set as 400ms, which indicates the normal state. The longest interval between two blinks is 6.8 seconds, person-dependent. Once the BD exceeds 900ms, the mental state of user could be considered as microsleep, which increases the risk level. Then, a blink interval should be monitored. Once the interval exceeds 6.8 seconds, eye closure is detected. This algorithm is illustrated in Fig. 38.

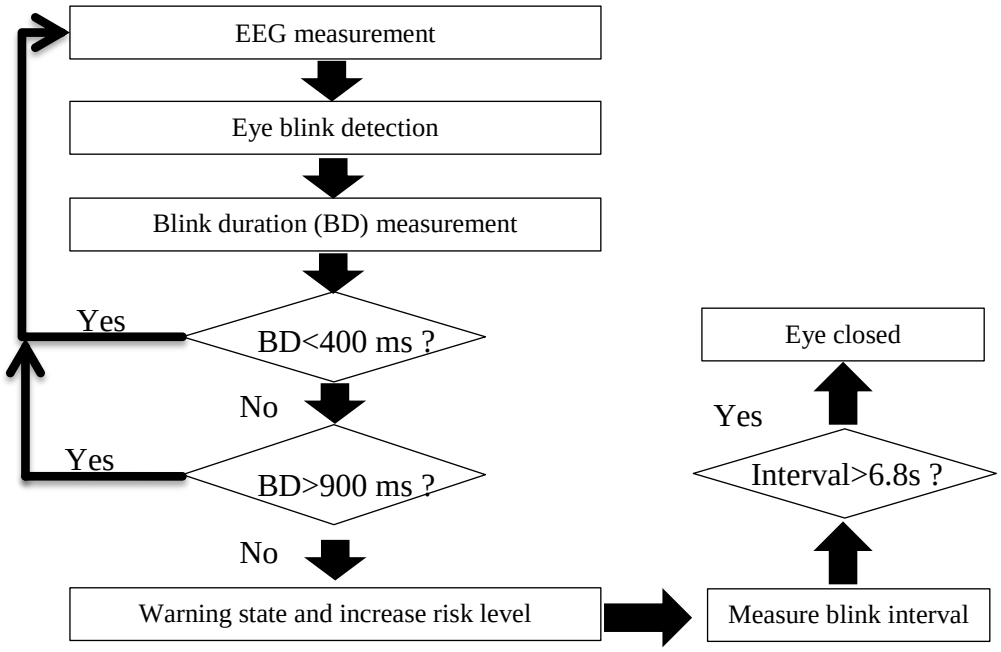

Figure 38. Algotithm of fatigue detection by eye blink

6.4 Summary and future work

The EEG signal could be measured by the SSH based on dry electrodes. A band pass filter is used to remove the noise in order to screen out the eye blink. The variance of EEG signal was used to locate the eye blink using a sliding window. Once the eye blink is detected, the parameters including the duration and interval is measured. These parameters are used to determine if the SSH user is in a fatigue state or a microsleep with increasing risk.

The parameters setting for detecting eye blink duration in the algorithm are based on the previous research works presented in literature review. Meanwhile, the algorithm needs a real time validation and improvement in the future. For example, we can use fuzzy logic in order to compute a level of fatigue using both eye blink and EEG frequency analysis. Using the same algorithm, we can combine head motion in order to compute a final risk level.

Chapter 7: Conclusion

Some mental states, such as fatigue or sleepiness, can increase accident risk possibility in industrial facility, since lack of concentration may cause misuse of machine and then cause injury to human. Meanwhile, numerous robotics applications are expanding in industry, so that the human safety in human-robot interaction plays an important role in robot research field.

In our research, we have developed an intelligent system using wearable system, aiming at detecting the risk of the workers in industrial facility. This system is centered on a Smart Safety Helmet containing several sensory such as IMU and EEG in order to track worker head motion and mental states.

A head motion vocabulary is defined by the acceleration signal including 12 basic motions. The Nodding off was considered representing the "risky" motion in industrial environment because it is normally caused by fatigue or drowsiness. Cross-correlation and neural network was used to classify and identify the motions.

Cross-correlation is used to compare spatial similarity between the references and new acquired data. In our algorithm, each head motion is represented by discrete acceleration series. For computation standardization, these discrete series are sorted into a histogram including 50 bins and ± 10 m/s^2 limits. Then, the acceleration distribution in bins is used in the cross-correlation algorithm. The result shows that it works to identify the "Nodding off" with acceleration data preprocessing by a high pass filter, but still be confused by some actions, such as "Yes". The reason of this confusion could come from the step that sort discrete acceleration signal into histogram, which break the temporal continuity of waveform. As a result, the different motions, which include the same distribution of discrete acceleration signals, will have a higher similarity score.

On the other hand, it got more failures when recognizing the test models from a different person based on the same reference models. This indicates that the motions are personalized. If we want to identify head motions of different persons, we have to collect more data to build a public reference models.

The cross-correlation algorithm takes longer time when a new acquired motion is compared to the 12 reference models. So it is not appropriate to implement this algorithem

in real time. Then, a neural network algorithm was exploited to classify the head motions. Offline analysis indicates that the multilayer perceptron has the capacity to identify the risky head motion, such as Nodding off, from other motions. After the offline training, it can be implemented in real time application.

Besides the accelerometer, with the help of magnetometer, a working scenario was simulated with initial orientation of the worker. The neural network algorithm can successfully identify the “look away”, and not depend on the specific head motion or posture. But the magnetometer also limit the real application condition, that means if we get the training data of one specific orientation, we have to perform the online experiment according to the same orientation. In the real working environment, this should not be a problem because the location of machine should be fixed and the normal orientation of worker should be known. With the “Max output” algorithm of neural network, the average accuracy of head motion recognition could achieve over 85% for single person validation.

As suggested in this research work, EEG signal could be measured by the dry electrodes. A band pass filter is used to remove the noise in order to screen out the eye blink. The variance of EEG signal was used to locate the eye blink event. Once the eye blink is detected, the parameters including the duration and interval is measured. These parameters, combining with the head motion, are used to determine if the SSH user is in dangerous state.

Future works

The challenge of head motion recognition comes from the segmentation of the signals. In our offline training, the local maxima and fixed data points are used to segment the acceleration signal, which caused some confusion in training results. In the future, this method should be optimized in order to improve the classification capability of the neural network algorithm.

The algorithm of eye blinks detection by EEG need to be validated online. This algorithm also needs to be optimized in order to avoid the EEG noise caused by inadequate contact and electromyogram (EMG) signal.

The SSH system has the capability to detect the fatigue by an anomalous head motion and the features of eye blink. A process of data fusion combining EEG signal with the IMU signal is able to enhance the identification accuracy of the mental states and human intention

recognition. When an anomalous state is detected, real-time assistance can be used to convey non-visual information to the user using haptic biofeedback (and biorhythm). Our SSH could be combined to a prediction of collision and collision avoidance algorithm when the process includes a robot. As well, the SSH also could be used by the truck driver, robot operator who needs interaction, as well as miner for fatigue detection.

Appendix A

Fig. 39 is the Certificate of research ethic, issued by UQAC

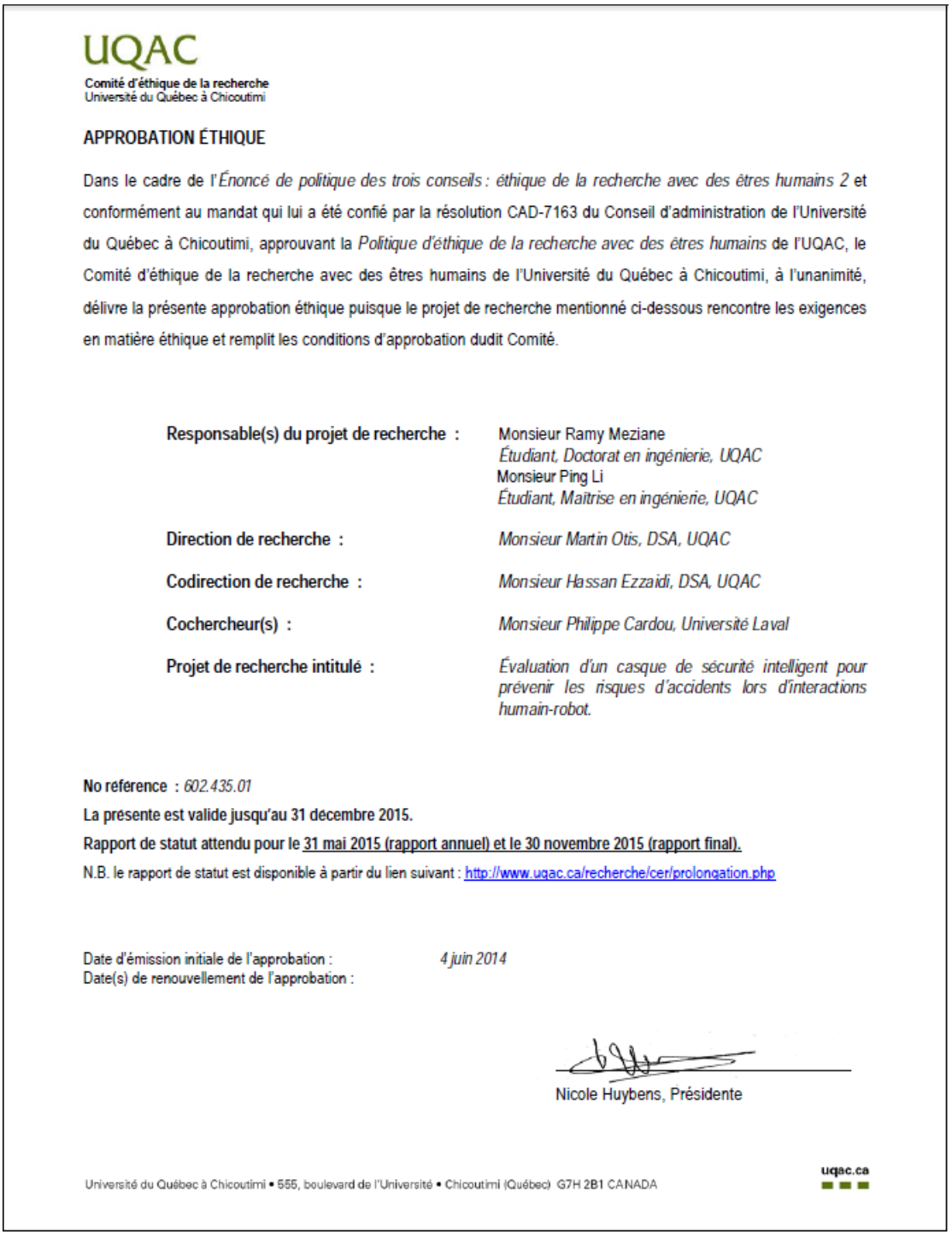

UQAC

Comité d'éthique de la recherche
Université du Québec à Chicoutimi

APPROBATION ÉTHIQUE

Dans le cadre de l'*Énoncé de politique des trois conseils : éthique de la recherche avec des êtres humains 2* et conformément au mandat qui lui a été confié par la résolution CAD-7163 du Conseil d'administration de l'Université du Québec à Chicoutimi, approuvant la *Politique d'éthique de la recherche avec des êtres humains* de l'UQAC, le Comité d'éthique de la recherche avec des êtres humains de l'Université du Québec à Chicoutimi, à l'unanimité, délivre la présente approbation éthique puisque le projet de recherche mentionné ci-dessous rencontre les exigences en matière éthique et remplit les conditions d'approbation dudit Comité.

Responsable(s) du projet de recherche :	Monsieur Ramy Meziane *Étudiant, Doctorat en ingénierie, UQAC* Monsieur Ping Li *Étudiant, Maîtrise en ingénierie, UQAC*
Direction de recherche :	*Monsieur Martin Otis, DSA, UQAC*
Codirection de recherche :	*Monsieur Hassan Ezzaidi, DSA, UQAC*
Cochercheur(s) :	*Monsieur Philippe Cardou, Université Laval*
Projet de recherche intitulé :	*Évaluation d'un casque de sécurité intelligent pour prévenir les risques d'accidents lors d'interactions humain-robot.*

No référence : *602.435.01*

La présente est valide jusqu'au 31 décembre 2015.

Rapport de statut attendu pour le 31 mai 2015 (rapport annuel) et le 30 novembre 2015 (rapport final).

N.B. le rapport de statut est disponible à partir du lien suivant : http://www.uqac.ca/recherche/cer/prolongation.php

Date d'émission initiale de l'approbation : *4 juin 2014*
Date(s) de renouvellement de l'approbation :

Nicole Huybens, Présidente

Université du Québec à Chicoutimi • 555, boulevard de l'Université • Chicoutimi (Québec) G7H 2B1 CANADA

uqac.ca

Figure 39. Certificate of research ethic

Appendix B

XBee setup for remotely controlled SSR

In the SSH end, IOIO firmware communicates with the XBee transmitter via UART (Universal Asynchronous Receiver/Transmitter). The “Remote AT Command” of XBee is used to transmit the On/Off signal to Xbee receiver. Fig. 40 illustrates the circuit design of this setup.

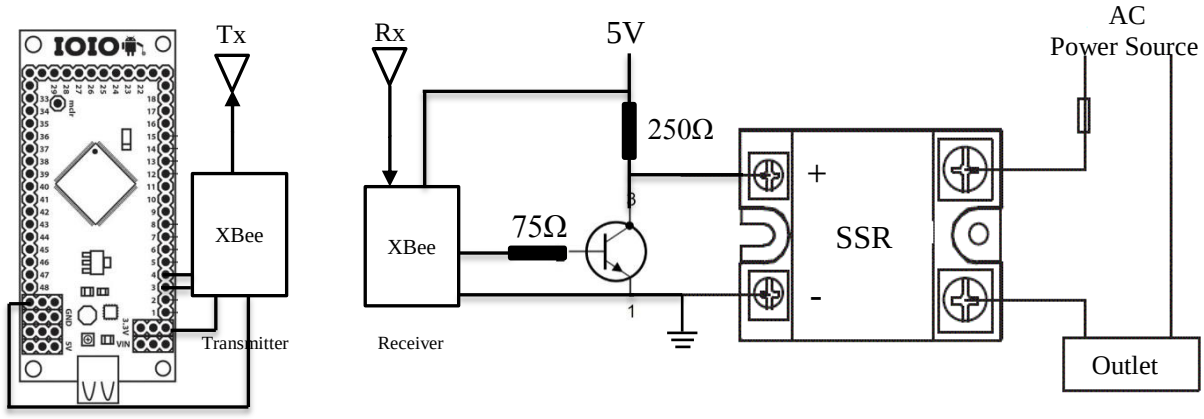

Figure 40. Xbee setup for remotely control SSR relay.

The frame-based API (Application Programming Interface) operation of Xbee extends the level to which a host application can interact with the networking capabilities of the module. When in API mode, all data entering and leaving the module's UART is contained in frames that define operations. “Remote AT Command” of Xbee is used to query or set module parameters on a remote device. The detailed description of this could be found in datasheet 90002134_C.pdf [70].

The API operation of Xbee is frame-based. The frame Type of “Remote AT Command request” is 0x17. With the help of Frame Maker, two frames of requesting the pin “D1” of Xbee receiver to output high and low is “7E 00 10 17 00 00 13 A2 00 40 A2 69 F7 FF FE 02 44 31 05 78” and “7E 00 10 17 00 00 13 A2 00 40 A2 69 F7 FF FE 02 44 31 04 79”. These data could be sent by our SSH (IOIO) via Xbee transmitter to the Xbee receiver. Normally, the output of D1 of receiver is LOW, that means the status of SSR is On and the power supply of the machine is normal. Once a high risk is detected, the D1 of Xbee receiver output High to cut off the power.

References

[1] M. Vasic, and A. Billard, “Safety Issues in Human-Robot Interactions,” in *2013 IEEE International Conference on Robotics and Automation*, Karlsruhe, Germany, 2013.

[2] Marty Albert, Retsch Toni, and G. Schmitter,"Safety Principles for Industrial Robots," 15-Feb, 2014; http://www.ilo.org/oshenc/part-viii/safety-applications/item/972-safety-principles-for-industrial-robots.

[3] Association of Workers’ Compensation Boards of Canada. "Number of Fatalities, by Occupation and Jurisdiction," 05 Mar, 2015; http://awcbc.org/?page_id=14#fatalities.

[4] T. Malm, J. Viitaniemi, J. Latokartano, S. Lind, O. Venho-Ahonen, and J. Schabel, “Safety of interactive robotics-learning from accidents,” *International Journal of Social Robotics*, vol. 2, no. 3, pp. 221-227, 2010.

[5] Occupational Safety and Health Administration. "INDUSTRIAL ROBOTS AND ROBOT SYSTEM SAFETY," 26-Feb, 2014; https://www.osha.gov/dts/osta/otm/otm_iv/otm_iv_4.html.

[6] I. 10218-1:2006, "Robots for industrial environments -- Safety requirements -- Part 1: Robot," 2006.

[7] C. S. Association, "Industrial Robots and Robot Systems - General Safety Requirements," 2003.

[8] F. J. Llorén s, L. M. Molina, and A. J. Verdú, “Flexibility of manufacturing systems, strategic change and performance,” *International Journal of Production Economics*, vol. 98, no. 3, pp. 273-289, 12/18/, 2005.

[9] A. De Santis, and B. Siciliano, “SAFETY ISSUES FOR HUMAN–ROBOT COOPERATION IN MANUFACTURING SYSTEMS,” *Tools and Perspectives in Virtual Manufacturing*, 2008.

[10] Canadian Centre for Occupational Health & Safety. "Fatigue," 20 Jan, 2014; http://www.ccohs.ca/oshanswers/psychosocial/fatigue.html.

[11] Civil Aviation Authority of New Zealand. "Fatigue," 20 Jan, 2014; http://www.caa.govt.nz/Publications/Vector/Vector_Articles/Fatigue_NovDec00News.pdf.

[12] A. Belyavin, and N. A. Wright, “Changes in electrical activity of the brain with vigilance,” *Electroencephalography and Clinical Neurophysiology*, vol. 66, no. 2, pp. 137-144, 1987.

[13] H. Yu, L.-C. Shi, and B.-L. Lu, “Vigilance Estimation Based on EEG Signals,” in *Proceedings of IEEE/ICME International Conference on Complex Medical Engineering (CME2007)*, 2007.

[14] R. B. Levin, *EEG based consciousness-alert monitoring system*, WO1999034865 A1, 1999.

[15] F. Sauvet, C. Bougard, M. Coroenne, L. Lely, P. Van Beers, M. Elbaz, M. Guillard, D. Leger, and M. Chennaoui, “In-Flight Automatic Detection of Vigilance States

Using a Single EEG Channel," *Biomedical Engineering, IEEE Transactions on*, vol. 61, no. 12, pp. 2840-2847, 2014.

[16] A. Picot, S. Charbonnier, and A. Caplier, "Monitoring drowsiness on-line using a single encephalographic channel," *Recent Advances in Biomedical Engineering*, pp. 145-164, 2009.

[17] H. J. Eoh, M. K. Chung, and S.-H. Kim, "Electroencephalographic study of drowsiness in simulated driving with sleep deprivation," *International Journal of Industrial Ergonomics,* vol. 35, no. 4, pp. 307-320, 2005.

[18] J. A. Stern, D. Boyer, and D. Schroeder, "Blink rate: a possible measure of fatigue," *Human Factors: The Journal of the Human Factors and Ergonomics Society,* vol. 36, no. 2, pp. 285-297, 1994.

[19] P. P. Caffier, U. Erdmann, and P. Ullsperger, "The spontaneous eye-blink as sleepiness indicator in patients with obstructive sleep apnoea syndrome-a pilot study," *Sleep Medicine,* vol. 6, no. 2, pp. 155-162, 2005.

[20] P. P. Caffier, U. Erdmann, and P. Ullsperger, "Experimental evaluation of eye-blink parameters as a drowsiness measure," *European journal of applied physiology,* vol. 89, no. 3-4, pp. 319-325, 2003.

[21] A. Godfrey, R. Conway, D. Meagher, and O. L. G, "Direct measurement of human movement by accelerometry," *Med Eng Phys,* vol. 30, no. 10, pp. 1364-86, Dec, 2008.

[22] C. C. Yang, and Y. L. Hsu, "A review of accelerometry-based wearable motion detectors for physical activity monitoring," *Sensors (Basel),* vol. 10, no. 8, pp. 7772-88, 2010.

[23] Y. Ohtaki, K. Sagawa, and H. Inooka, "A method for gait analysis in a daily living environment by body-mounted instruments," *JSME International Journal Series C,* vol. 44, pp. 1125-1132, 2001.

[24] S. J. M. Bamberg, A. Y. Benbasat, D. M. Scarborough, D. E. Krebs, and J. A. Paradiso, "Gait analysis using a shoe-integrated wireless sensor system," *IEEE Transactions on Information Technology in Biomedicine,* vol. 12, no. 4, pp. 413-423, 2008.

[25] F. Zampella, M. Khider, P. Robertson, and A. Jiménez, "Unscented Kalman filter and Magnetic Angular Rate Update (MARU) for an improved Pedestrian Dead-Reckoning," in *IEEE/ION Position, Location and Navigation Symposium*, Myrtle Beach, SC, 2012, pp. 129-139.

[26] T. Gadeke, J. Schmid, M. Zahnlecker, W. Stork, and K. D. Muller-Glaser, "Smartphone pedestrian navigation by foot-IMU sensor fusion," in *Ubiquitous Positioning, Indoor Navigation, and Location Based Service*, 2012, pp. 1-8.

[27] M. Angermann, P. Robertson, T. Kemptner, and M. Khider, "A high precision reference data set for pedestrian navigation using foot-mounted inertial sensors," in *International Conference on Indoor Positioning and Indoor Navigation (IPIN)*, Zürich, Switzerland, 2010, pp. 1-6.

[28] S. Wan, and E. Foxlin, "Improved pedestrian navigation based on drift-reduced MEMS IMU chip," in *Proceedings of the 2010 International Technical Meeting of The Institute of Navigation*, San Diego, CA, 2010, pp. 220-229.

[29] C. Smith, and H. I. Christensen, “Wiimote robot control using human motion models,” in *IEEE/RSJ International Conference on Intelligent Robots and Systems*, 2009, pp. 5509-5515.

[30] G. Pang, and H. Liu, “Evaluation of a low-cost MEMS accelerometer for distance measurement,” *Journal of Intelligent and Robotic Systems: Theory and Applications*, vol. 30, no. 3, pp. 249-265, 2001.

[31] C. S. a. H. I. Christensen, “Wiimote Robot Control Using Human Motion Models,” 2009.

[32] J. Liu, L. Zhong, J. Wickramasuriya, and V. Vasudevan, “uWave: Accelerometer-based personalized gesture recognition and its applications,” *Pervasive and Mobile Computing*, vol. 5, no. 6, pp. 657-675, 2009.

[33] Y. Zhou, L. Jing, J. Wang, and Z. Cheng, “Analysis and Selection of Features for Gesture Recognition Based on a Micro Wearable Device,” *International Journal of Advanced Computer Science & Applications*, vol. 3, no. 1, 2012.

[34] C. Zhu, and S. Weihua, “Human daily activity recognition in robot-assisted living using multi-sensor fusion,” in *IEEE International Conference on Robotics and Automation*, 2009, pp. 2154-2159.

[35] C. Marselli, D. Daudet, H. P. Amann, and F. Pellandini, "Application of Kalman filtering to noise reduction on microsensor signals." pp. 443-450.

[36] J. A. Corrales Ramón, F. A. Candelas Herías, and F. Torres Medina, “Kalman filtering for sensor fusion in a human tracking system,” 2010.

[37] M. S. Grewal, and A. P. Andrews, *Kalman filtering: theory and practice using MATLAB*: Wiley. com, 2011.

[38] E. Foxlin, “Pedestrian tracking with shoe-mounted inertial sensors,” *IEEE Computer Graphics and Applications*, vol. 25, no. 6, pp. 38-46, //, 2005.

[39] E. F. Sheng Wan, “Improved Pedestrian Navigation Based on Drift-Reduced MEMS IMU Chip,” 2010.

[40] E. M. Foxlin, “Inertial head-tracker sensor fusion by a complementary separate-bias Kalman filter,” in *Proceedings of the IEEE Virtual Reality Annual International Symposium*, 1996, pp. 185-194, 267.

[41] E. M. Foxlin, M. Harrington, and Y. Altshuler, “Miniature six-DOF inertial system for tracking HMDs,” in *Aerospace/Defense Sensing and Controls*, 1998, pp. 214-228.

[42] H. B. Menz, S. R. Lord, and R. C. Fitzpatrick, “Acceleration Patterns of the Head and Pelvis When Walking Are Associated With Risk of Falling in Community-Dwelling Older People,” *The Journals of Gerontology Series A: Biological Sciences and Medical Sciences*, vol. 58, no. 5, pp. M446-M452, May 1, 2003, 2003.

[43] A. Pajkanović, and B. Dokić, “Wheelchair control by head motion,” *Serbian Journal of Electrical Engineering*, vol. 10, no. 1, pp. 135-151, 2013.

[44] O. D. Lara, and M. A. Labrador, “A survey on human activity recognition using wearable sensors,” *Communications Surveys & Tutorials, IEEE*, vol. 15, no. 3, pp. 1192-1209, 2013.

[45] E. Nelson-Wong, S. Howarth, D. A. Winter, and J. P. Callaghan, “Application of autocorrelation and cross-correlation analyses in human movement and

rehabilitation research," *journal of orthopaedic & sports physical therapy*, vol. 39, no. 4, pp. 287-295, 2009.

[46] S. W. Smith, "The Scientist and Engineer's Guide to Digital Signal Processing," California Technical Publishing, 1999.

[47] R. Y. W. Lee, and T. K. T. Wong, "Relationship between the movements of the lumbar spine and hip," *Human Movement Science,* vol. 21, no. 4, pp. 481-494, 2002.

[48] T. A. L. Wren, K. Patrick Do, S. A. Rethlefsen, and B. Healy, "Cross-correlation as a method for comparing dynamic electromyography signals during gait," *Journal of Biomechanics,* vol. 39, no. 14, pp. 2714-2718, 2006.

[49] J.-S. Wang, and C. Fang-Chen, "An Accelerometer-Based Digital Pen With a Trajectory Recognition Algorithm for Handwritten Digit and Gesture Recognition," *Industrial Electronics, IEEE Transactions on,* vol. 59, no. 7, pp. 2998-3007, 2012.

[50] C. Zhu, and S. Weihua, "Online hand gesture recognition using neural network based segmentation," in *Intelligent Robots and Systems, 2009. IROS 2009. IEEE/RSJ International Conference on*, 2009, pp. 2415-2420.

[51] A. Picot, S. Charbonnier, and A. Caplier, "On-line automatic detection of driver drowsiness using a single electroencephalographic channel." pp. 3864-3867.

[52] A. Delorme, T. Sejnowski, and S. Makeig, "Enhanced detection of artifacts in EEG data using higher-order statistics and independent component analysis," *NeuroImage,* vol. 34, no. 4, pp. 1443-1449, 2007.

[53] C. A. Joyce, I. F. Gorodnitsky, and M. Kutas, "Automatic removal of eye movement and blink artifacts from EEG data using blind component separation," *Psychophysiology,* vol. 41, no. 2, pp. 313-325, 2004.

[54] M. Viqueira, B. G. Zapirain, and A. M. Zorrilla, "Ocular Movement and Cardiac Rhythm Control using EEG Techniques," *Medical Imaging in Clinical Practice*, 2013.

[55] T. Danisman, I. M. Bilasco, C. Djeraba, and N. Ihaddadene, "Drowsy driver detection system using eye blink patterns," in *Machine and Web Intelligence (ICMWI), 2010 International Conference on*, 2010, pp. 230-233.

[56] J. Qiang, Z. Zhiwei, and P. Lan, "Real-time nonintrusive monitoring and prediction of driver fatigue," *Vehicular Technology, IEEE Transactions on,* vol. 53, no. 4, pp. 1052-1068, 2004.

[57] G. Li, and W.-Y. Chung, "Estimation of Eye Closure Degree Using EEG Sensors and Its Application in Driver Drowsiness Detection," *Sensors,* vol. 14, no. 9, pp. 17491-17515, 2014.

[58] R. N. Roy, S. Charbonnier, and S. Bonnet, "Eye blink characterization from frontal EEG electrodes using source separation and pattern recognition algorithms," *Biomedical Signal Processing and Control,* vol. 14, pp. 256-264, 2014.

[59] B. Chambayil, R. Singla, and R. Jha, "EEG eye blink classification using neural network," in *Proceedings of the World Congress on Engineering*, 2010, pp. 2-5.

[60] T. Cao, F. Wan, C. Wong, J. da Cruz, and Y. Hu, "Objective evaluation of fatigue by EEG spectral analysis in steady-state visual evoked potential-based brain-computer interfaces," *BioMedical Engineering OnLine,* vol. 13, no. 1, pp. 28, 2014.

[61] T. O. Zander, M. Lehne, K. Ihme, S. Jatzev, J. Correia, C. Kothe, B. Picht, and F. Nijboer, "A dry EEG-system for scientific research and brain-computer interfaces," *Frontiers in Neuroscience*, vol. 5, 2011-May-26, 2011.

[62] O. R. Inc.,Orbital Research Inc. "SilverBumps Electrodes Specification," February 16, 2014; http://orbitalresearch.com/PDFs/Orbital_Dry_Electrode_Spec_Sheet.pdf.

[63] M. Teplan, "Fundamentals of EEG measurement," *Measurement science review*, vol. 2, no. 2, pp. 1-11, 2002.

[64] Bitalino,"Sensor: Electrocardiography (ECG)," 6-Jan, 2015; http://store.bitalino.com/index.php/standard-account-store#!/Electrocardiography-ECG/p/44963155/category=11569758.

[65] Ytai,"IOIO wiki," https://github.com/ytai/ioio/wiki.

[66] J. Heaton,"Encog Machine Learning Framework," 04-Sep, 2014; http://www.heatonresearch.com/encog.

[67] T. Canada,"Road Safety in Canada," 03-Feb, 2015; http://www.tc.gc.ca/eng/motorvehiclesafety/tp-tp15145-1201.htm#s34.

[68] C.-S. Hsieh, and C.-C. Tai, "AN IMPROVED AND PORTABLE EYE-BLINK DURATION DETECTION SYSTEM TO WARN OF DRIVER FATIGUE," *Instrumentation Science & Technology*, vol. 41, no. 5, pp. 429-444, 2013/09/03, 2013.

[69] R. Schleicher, N. Galley, S. Briest, and L. Galley, "Blinks and saccades as indicators of fatigue in sleepiness warnings: looking tired?," *Ergonomics*, vol. 51, no. 7, pp. 982-1010, 2008/07/01, 2008.

[70] D. International,"XBee-PRO® 900 RF Modules," http://ftp1.digi.com/support/documentation/90002134_C.pdf.